DOKUZ EYLÜL UNIVERSITY

GRADUATE SCHOOL OF NATURAL AND APPLIED SCIENCES

EVALUATION OF PHOSPHORUS RECOVERY AS VIVIANITE

by

Seda KARABACAKOĞULLARI

October, 2022

İZMİR

EVALUATION OF PHOSPHORUS RECOVERY AS VIVIANITE

A Thesis Submitted to the
Graduate School of Natural and Applied Sciences of Dokuz Eylül University
In Partial Fulfillment of the Requirements for the Degree of Master of Science in Environmental Engineering

by
Seda KARABACAKOĞULLARI

October, 2022
İZMİR

M.Sc. THESIS EXAMINATION RESULT FORM

We have read the thesis entitled **"EVALUATION OF PHOSPHORUS RECOVERY AS VIVIANITE"** completed by **SEDA KARABACAKOĞULLARI** under supervision of **PROFESSOR DOCTOR NURDAN BÜYÜKKAMACI** and we certify that in our opinion it is fully adequate, in scope and in quality, as a thesis for the degree of Master of Science.

Prof.Dr. Nurdan BÜYÜKKAMACI

Supervisor

Prof.Dr. Ayşe FİLİBELİ

(Jury Member)

Assoc. Prof. Dr. Nazlı BALDAN PAKDİL

(Jury Member)

Prof. Dr. Okan FISTIKOĞLU

Director

Graduate School of Natural and Applied Sciences

ACKNOWLEDGEMENTS

I would first like to thank my thesis supervisor, Prof. Dr. Nurdan BÜYÜKKAMACI, for her excellent support and knowledge. I am deeply grateful to Instructor Duygu Totur PAMIK and Env.Eng. Yaren ZÜMRÜT for their valuable support on experimental studies.

I also thank the Research Foundation of Dokuz Eylul University (Project No: 2021.KB.FEN.045) for financial support.

Finally, I would like to thank my lovely family for always being there.

Seda KARABACAKOĞULLARI

EVALUATION OF PHOSPHORUS RECOVERY AS VIVIANITE

ABSTRACT

Phosphorus is essential for all living things and its recovery is a vital issue for the world. Existing practices have limitations in terms of efficiency and applicability and more economical and efficient phosphate recovery techniques are needed. If iron and phosphate are present and relatively less sulphide concentrations are present, vivianite an iron phosphate mineral, is formed in anaerobic conditions. Vivianite is a valuable mineral used in some industrial facilities and agricultural activities. Therefore, recovery of phosphorus from wastewater based on vivianite formation not only contributes to the sustainable use of phosphorus, but also provides potential economic opportunities.

In this study, it was aimed to determine the recovery potential of phosphorus as vivianite and to evaluate the effects of operational conditions on phosphorus recovery. For this purpose, lab-scale semi-batch completely mixed crystallizer reactor (CSTR) was first used. After then, a lab-scale fluidized bed reactor (FBR) was operated based on the results obtained from the CSTR. Sodium phosphate solution and iron chloride solution was used as a phosphorus containing synthetic wastewater and as an iron source, respectively. In CSTR studies, the effects of pH, Fe:P ratio, Fe feeding rate, and P concentration for vivianite crystallization were investigated. In FB studies, the effect of seed material, P concentration, and recycle ratio was examined. As a result of all experimental studies, vivianite formation was observed in both reactors and confirmed by SEM, XRD, SEM-EDS analyzes. P removal efficiencies of up to 50-69% has been achieved by vivianite crystallization. No precipitation was observed when the phosphorus concentration fell below 50 mg/L. Therefore, it was determined that wastewater with a high phosphorus concentration is more suitable for vivianite crystallization.

Keywords: Phosphorus, recovery, vivianite, crystallization, wastewater

FOSFORUN VİVİANİT OLARAK GERİ KAZANIMININ DEĞERLENDİRİLMESİ

ÖZ

Fosfor tüm canlılar için çok önemli bir elementtir ve geri kazanımı tüm Dünya için hayati öneme sahip bir konudur. Mevcut uygulamaların verimlilik ve uygulanabilirlik açısından sınırlamaları vardır ve bu nedenle, daha ekonomik ve verimli fosfat geri kazanım tekniklerine ihtiyaç duyulmaktadır. Demir, fosfat ve nispeten daha az sülfür konsantrasyonları mevcutsa, anaerobik koşullarda bir demir fosfat minerali olan vivianit oluşur. Vivianit, bazı endüstriyel tesislerde ve tarımsal faaliyetlerde kullanılan değerli bir mineraldir. Bu nedenle atıksudan vivianit oluşumuna dayalı fosfor geri kazanımı, sadece fosforun sürdürülebilir kullanımına katkı sağlamakla kalmayıp, aynı zamanda potansiyel ekonomik fırsatlar da sağlayacaktır.

Bu çalışmada fosforun vivianit olarak geri kazanım potansiyelinin belirlenmesi ve işletme koşullarının fosfor geri kazanımına etkilerinin değerlendirilmesi amaçlanmıştır. Öncelikle laboratuvar ölçekli yarı kesikli sürekli karıştırmalı kristalizatör (CSTR) kullanılmıştır. Çalışmanın devamında CSTR sisteminde elde edilen sonuçlara göre çalıştırılan akışkan yataklı kristalizatör (FB) kullanılmıştır. Deneysel çalışmalarda sentetik atıksu olarak sodyum hidrojen fosfat içeren çözelti ve demir kaynağı olarak demir klorür çözeltisi kullanılmıştır. CSTR çalışmalarında, pH, Fe:P oranı, Fe besleme hızı ve P konsantrasyonunun vivianit kristalizasyonuna etkileri araştırılmıştır. FB denemelerinde aşı malzeme, P konsantrasyonu ve geri devir oranının etkisi incelenmiştir. Deneysel çalışmalar sonucunda, her iki reaktörde de vivianit oluşumu gözlemlenmiştir ve vivianit oluşumu SEM, XRD, SEM-EDS analizleri ile doğrulanmıştır. Vivianit kristalizasyonu ile %50-69'a varan P giderme verimleri elde edilmiştir. 50 mg/L'den daha az P konsantrasyonlarında çökelek oluşumu gözlenmediğinden, vivianit kristalizasyonunun yüksek P konsantrasyonuna sahip atıksular için daha uygun olduğu belirlenmiştir.

Anahtar kelimeler: Fosfor, geri kazanım, vivianit, kristalleşme, atıksu

CONTENTS

Page

LIST OF FIGURES

LIST OF TABLES

LIST OF SYMBOLS

^0C	Celsius degree
Δ	Delta
μ	Dynamic viscosity
ϑ	Velocity
ε	Void fraction
φ	Sphericity

ABBREVIATIONS

DNA	Deoxyribo Nucleic Acid
RNA	Ribonucleic Acid
NPK	Nitrogen, Phosphorus and Potassium
PAO	Phosphate Accumulating Organisms
VFA	Volatile Fatty Acids
AO	Anaerobic/Oxic
A^2O	Anaerobic/Anoxic/Oxic
RAS	Return Activated Sludge
EBPR	Enhanced Biological P Removal
MAP	Magnesium Ammonium Phosphate
HAP	Hydroxyapatite
DMRB	Dissimilatory Metal-Reducing Bacteria
K_{sp}	Solubility Constant
SRB	Sulfate-Reducing Bacteria
CSTR	Continuous Stirred-Tank Reactor
FB	Fluidized Bed
FBR	Fluidized Bed Reactor
XRD	X-Ray Diffraction
SEM	Scanning Electron Microscope
SEM-EDS	Scanning Electron Microscopy Energy Dispersive Spectroscopy

CHAPTER 1
INTRODUCTION

1.1 Phosphorus Element

Phosphorus is an essential element for all living things. Its main characteristics are given in Table 1.1 (Royal Society of Chemistry, 2022).

Table 1.1 Properties of phosphorus

Group	5-A
Period	3
Block	p
Atomic number	15
State at 20°C	Solid
Electron configuration	[Ne] $3s^2 3p^3$
Melting point	44.15°C
Boiling point	280.5°C
Density (g cm^{-3})	1.823 (white)
Relative atomic mass	30.974
CAS number	7723-14-0

Phosphorus is critical element, which is found in DNA, RNA and all vital cells in the body and essential nutrient for production of food and feed. In the absence of phosphorus, there has no food production and cell growth. “Unlike the other fundamental elements underpinning life (carbon, nitrogen, oxygen and hydrogen), phosphorus has no significant gaseous phase and cannot circulate freely in the atmosphere” (Cordell and White, 2011).

Phosphorus is used in the production of many products, and it is necessary for continuity of life. Figure 1.1 describes the end uses of phosphorus by percentage. The biggest portion is for agricultural uses to produce food.

Industrial uses are involved such as detergents, personal care products, pharmaceuticals, and other industrial applications. Global phosphorus shortage is a big threat for the world. Many scientific articles are agreed that the world has phosphorus for 50-100 years. However, estimates of a lifetime of current world phosphate reserves differ by different authors. For example, depletion time estimates as 300-400 years by some authors (Cordell and White, 2011).

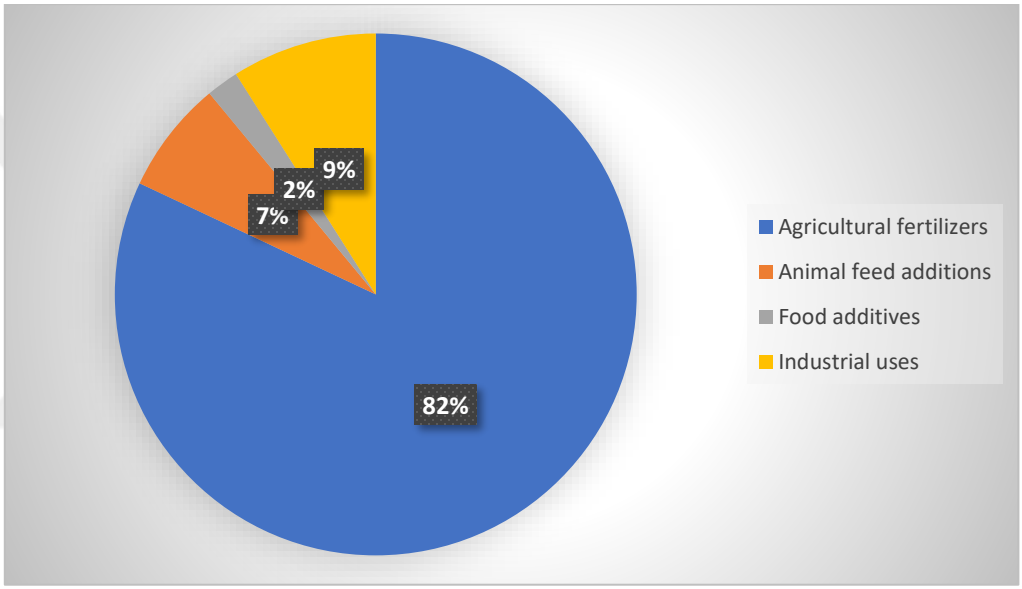

Figure 1.1 Distribution of phosphorus end uses (Schröder et al., 2006)

Despite all the research and different estimates, it is an undeniable fact that phosphorus sources are exhausted and there is no other source that can be used or synthesized instead of phosphorus.

Chemist and science writer Isaac Asimov described phosphorus as “life’s bottleneck” and warned 30 years ago, “We may be able to substitute nuclear power for coal, and plastics for wood, and yeast for meat, and friendliness for isolation but for phosphorus there is neither substitute nor replacement” (Cordell and White, 2014).

The remaining phosphorus will not have as high phosphorus content of phosphorus as the previous reserves.

Phosphorus levels are not sufficient, and the heavy metal content is expected to be high. Difficulty accessing the phosphorus mine and the decrease in its quality will affect mining activities and will not make this process economically viable.

On the other hand, there are serious environmental concerns about phosphorus rock mining. Mining itself has important damaging effects in natural resources such water, soil, and air. In phosphate rock mining case, these damaging effects can be seen in chemical processing step of mining. For example, drastic chemical processing with strong acids are necessary to produce soluble phosphate products from apatite, which is the mostly abundant phosphate mineral (Reta et al., 2018).

1.2 Phosphorus Reserves

Phosphorus is found mostly as salts of phosphoric acid. It is obtained from minerals containing phosphate. There are about 200 different mineral phosphorus. The most important of these minerals is "apatite" mineral. Other phosphate-containing minerals: vivianite, pyromorphite, vavellite, variskite, etc.

The total reserve of phosphate deposits in the world is estimated to be 50 billion tons. Production of phosphorus minerals changes between 150-200 million tons per year. There are phosphate deposits in the USA, Russia, Morocco, Tunisia, Algeria, Jordan, Israel, Senegal, Togo, Gabon, South Africa, Indian, and Pacific islands. Figure 1.2 shows the remaining phosphate rock reserves. Considering the distribution of phosphorus in the world, it is not possible to talk about an even distribution. Given this distribution, efficient use and reuse of phosphorus are very important, as it is an essential and vital element (Eskier, 2017).

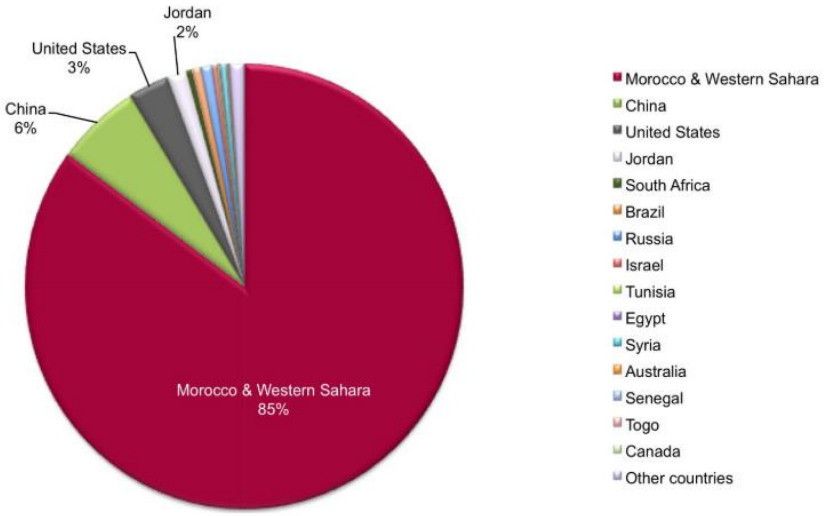

Figure 1.2 Remaining global phosphate rock reserves as reported in 2010 by International Fertilizer Development Center (IFDC).

In Turkey, it is also found in phosphate beds Southeastern Anatolia. There are phosphate deposits in Bingöl (Genç, Ünaldı), Adıyaman (Çelikhan, Tut, Besni), Hatay (Yayladağı), Kilis and Şanlıurfa (Bozora) regions, especially in Mazıdağı and Mardin regions (Eskier, 2017). Mazıdağı, which is close to phosphate, one of the main ingredients of fertilizers, is in the Mardin region. In our country, phosphate is an important mineral used in 85-90% fertilizer, 10-15% feed, food, chemical and detergent industries ("Fosfat Kayası", 2022).

At the phosphorus usage in our country fertilizer area has the biggest portion. However, we don't have raw materials to produce fertilizer. In the raw material case, our country at least 80% is foreign dependent (TAGEM, Gübre Sektör Politika Belgesi, 2018-2022). Phosphorus usage amount, consumption amount, and needed amount and increase over the years. It is estimated to be an upward trend. To meet the needs, phosphorus production and import are foreseen to continue.

Phosphorus production and consumption amounts from 2013 to 2017 in Turkey is given in Table 1.2. When the table is examined, it is seen that there is an increase in the

consumption amount of phosphorus. This is an inevitable consequence due to the increasing population of the country. Increase in consumption brought along an increase in production.

Table 1.2 Phosphorus amount in Turkey (ton)

Year	Amount of production	Amount of consumption
2013	190.113,54	271.906,62
2014	212.935,09	248.965,23
2015	225.308,28	255.222,61
2016	215.185,14	246.001,07
2017	390.670,00	423.000,00

The increase in the production of fertilizer does not change the reality of Turkey dependent on raw material for the production. Since the raw materials used in fertilizer production are imported, fertilizer prices depend on exchange rates.

Factors such as the increasing population of the country, increase in food requirements, and decrease in arable land per person is reflected in the market as an increase in fertilizer consumption and therefore in need. Due to the depreciation of the Turkish lira against the dollar, fertilizer prices increased 142%- 152% in the first eight months of 2018. Fertilizers and plant nutrients must be used to obtain more products per unit area with today's technical possibilities. Countries that feed their plants well also feed their animals and people well.

Today, 550 kg pure NPK (nitrogen, phosphorus, and potassium) is used per hectare in agriculture in the Netherlands, 235 kg in Germany, 190 kg in Greece, while only 95 kg pure NPK is used in our country ("ZMO: Ülkemizde Gübre Üretimi ve Tüketimi Üzerine Bir Değerlendirme", 2022). The amount of fertilizer a fundamental factor for efficient agriculture and our country lag other countries in this regard.

CHAPTER 2
PHOSPHORUS IN WASTEWATER TREATMENT PLANTS

2.1 Phosphorus in Wastewater

Phosphorus is found in water as phosphate. Controlled discharge of phosphorus is important to prevent eutrophication in surface waters. Eutrophication threatens aquatic life as well as causes it to end completely. Mainly, there are three types of phosphate: orthophosphate, polyphosphate, and organic phosphate. Body and food wastes are sources of organic phosphate, yet some industrial sources can contain organic phosphate. Orthophosphate is an inorganic and soluble form of phosphate. 70-90% of total phosphorus in wastewater accounts for orthophosphate (Curtin et al., 2011). Polyphosphate is another inorganic form of phosphate, which is derived from synthetic detergents. Total phosphorus in the wastewater streams is the sum of all phosphate types. Table 2.1 summarizes different phosphate forms and their typical concentration in domestic wastewater.

Table 2.1 Phosphorus in domestic wastewater (Curtin et al., 2011)

Phosphate Form	Typical concentration (mg/L)
Orthophosphate	3.0 - 4.0
Na_3PO_4	
Na_2HPO_4	
NaH_2PO4	
$(NH_4)_2HPO_4$	
Polyphosphates	2.0 - 3.0
$Na_3(PO_3)_6$	
$Na_5P_3O_{10}$	
$Na_4P_2O_7$	
Organic Phosphates	0.7 - 1.0
Total as P	5.7 - 8.0

Human waste and synthetic detergents are the main sources of phosphorus in domestic wastewater. 50-60% and 30-50% of P comes from human waste and synthetic detergents, respectively (Doğan, 2010). Today, the increase in the use of synthetic detergents and the replacement of soaps by synthetic detergents have led to an increment in the amount of phosphorus in domestic wastewater. Discharge limits of urban wastewater treatment plants are 2 mg/L P for 10,000-100,000 equivalent population and 1 mg/L for higher than 100000 equivalent population (Kentsel Atıksu Arıtım Yönetmeliği, 2006).

According to the Republic of Turkey Presidency Legislation Information System Water Pollution Regulation, the sectors in which phosphorus is included in the discharge standards are listed below:

- Food industry (Bovine, small cattle breeding, and poultry houses)
- Thermal Power Plants
- Fertilizer production from phosphoric acid and / or phosphorous rock
- Plastic material production and processing of plastic materials
- Detergent Production
- Biodiesel facilities

When the discharge standards in these sectors are examined, it is seen that the concentration of phosphorus or phosphorus compounds changes between 1-2 mg/L. For example, while the discharge standard for a 2-hour composite sample in detergent production is 2 mg/L, this value drops to 1 mg/L for a 24-hour composite sample. The same discharge standards have been set for phosphorus for small and large organized industrial side wastewater for which no sector determination has been made.

When the quality criteria of inland water resources are examined based on phosphorus parameter, 0.02 mg/L for first-class water quality, 0.16 mg/L for second-class water quality, 0.65 mg/L for third-class water quality and higher values than 0.65 mg/L for fourth-class water quality concentration is stated as limit values (Su Kirliliği Kontrolü Yönetmeliği, 2004).

2.2 Phosphorus Treatment

Phosphorus treatment is a key factor for preventing eutrophication and protecting the ecosystem. Both discharge standards of phosphorus and its vital effect on the environment need efficient phosphorus removal. Widely applied phosphorus removal methods are chemical and enhanced biological processes.

2.2.1 Biological Phosphorus Treatment

Biological phosphorus removal processes are widely used methods. Phosphorus can be separated from wastewater by special microorganisms called phosphate accumulating organisms (PAOs). These microorganisms can store excess phosphate, which more than their own biological growth in anaerobic conditions. An adequate amount of PAOs is essential for a successful phosphorus treatment. Mechanisms of biological phosphorus uptake is summarized in Figure 2.1. Anaerobic and aerobic zones are essential for phosphorus removal from wastewater. VFAs are occurred by fermentation of organics and play an important role in the anaerobic zone. Amount of volatile fatty acids (VFA) and PAOs are strictly correlated with each other since VFAs affect PAOs growth. The biological phosphorus removal process removes 7 to 10 mg of VFAs for each mg of P that is removed. If enough VFAs are not produced naturally, chemical addition may be required to ensure adequate PAO population for optimum biological phosphorus removal (Curtin et al., 2011).

In anaerobic conditions, PAOs have stored polyphosphate as an energy source. Breakdown of polyphosphate molecules into orthophosphate releases energy. Orthophosphate molecules cannot be able to pass through the cell membranes due to their negative charge. They bond cations mainly potassium and magnesium to neutralize. Neutralized molecules can pass through the cell membrane and phosphorus release occurs. In aerobic conditions, more phosphate is absorbed than is released in anaerobic conditions.

As a result, P concentration in wastewater decreases at the end of the aerobic period (Dorofeev et al., 2020).

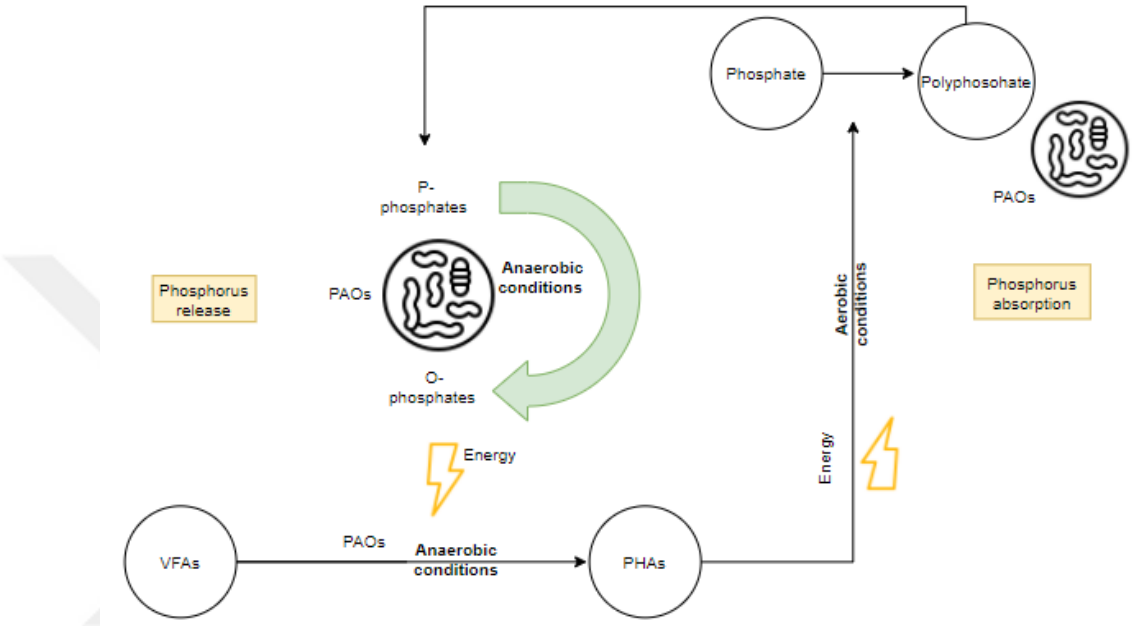

Figure 2.1 Mechanisms of biological phosphorus uptake (Dorofeev et al., 2020)

There are many different biological phosphorus removal (BPR) processes such as Anaerobic/Oxic (A/O design), Anaerobic/Anoxic/Oxic (A^2O design), Modified Bardenpho Design, and UCT design. Among them, A/O process is the basic biological P removal method. The schematic representation of A/O process is shown in Figure 2.2. The influent wastewater first passes into the anaerobic zone. In anaerobic conditions, the PAOs release phosphorus while accumulating and storing carbohydrates. The anaerobic zone is followed by an aerobic zone, where the PAOs consume the stored carbohydrates while taking up excess phosphorus (Technologies, 2022).

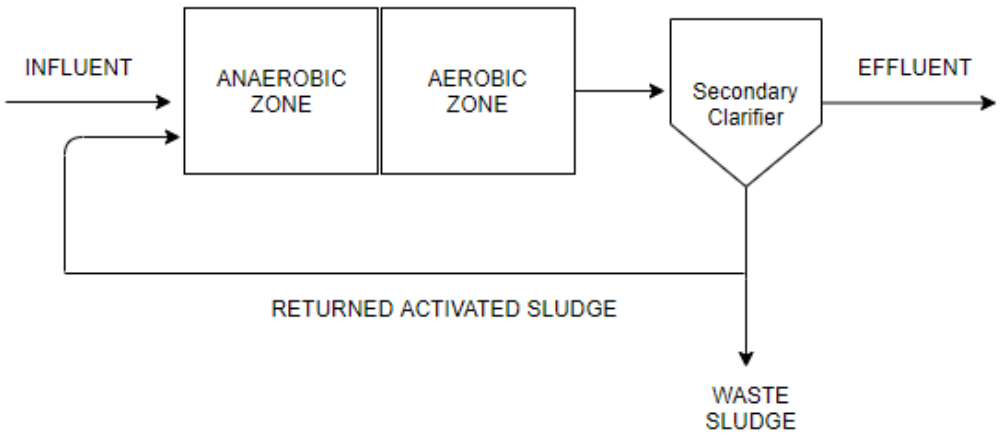

Figure 2.2 Schematic representation of basic BPR (Curtin et al., 2011).

2.2.2 Chemical Phosphorus Treatment

Chemical phosphorus removal can be achieved by adding coagulants to the wastewater. These coagulants are multivalent metal ions such as aluminum, iron, and calcium. Chemical phosphorus removal is easy to operate. However, sludge production is higher than biological methods. Increment in sludge production causes additional maintenance and cost.

Chemical treatment process includes rapid mixing (coagulation), slow mixing (flocculation), and sludge separation such as sedimentation, filtration, and membrane separation. Low P concentration, which may be less than 0.1 mg /L, can be achieved with chemical treatment. The type and dose of chemicals, pH, temperature, and mixing intensity are the main important operating factors. As a result of the process, significant amount of sludge produce that must be processed through dewatering and disposal. The reactions consume a significant amount of alkalinity (Hill, 2011).

2.2.3 Current Phosphate Treatment Techniques

In today's conditions, it can not be said that every facility works with good efficiency in phosphorus treatment. Increasing the efficiency of phosphorus removal is important both environmentally and economically. Considering the phosphorus scarcity in the world, wastewater treatment plants are an important source of phosphorus. Wu et al. (2019) reported that recovering P from the wastewater could meet 15-20% of the overall demand.

Existing phosphorus recovery techniques are not sufficient due to low yield and application difficulties. While the recovery rate from sludge and ash reaches 90%, the recovery rate from the liquid phase is at most 50% (Cornel and Schaum, 2009). Phosphorus recovery from sewage sludge, which has a high recovery efficiency, cannot be widely applied because it requires expensive special incineration plants. Another proposed technique, the recovery of phosphorus as struvite, has a yield of only 10-50% (Wilfert et al., 2018).

CHAPTER 3
PHOSPHORUS RECOVERY

3.1 Phosphorus Recovery Potential at WWTP

Phosphorus is an essential element for the continuation of life on earth. The absence of phosphorus means that there will be no fertilizer necessary for the growth of plants consumed as food. Since phosphorus resources are limited, optimal management of available phosphorus is essential and for this, recovery must be implemented. However, high phosphorus recovery is not easy. Recovery efficiency depends on several factors such as the amount of phosphorus, infrastructure of the wastewater treatment plant, and cost.

Each recovery technique has some advantages and disadvantages. Recovery from ash is 5-10 times higher than sludge and leachate. However, recovery from ash cannot be applied in every facility as it is costly. This application is more suitable for large WWTPs. Three possibilities for phosphorus recovery in wastewater treatment plant are listed below:

1. Use of sludge in agriculture directly: Since there is risk of the presence of organic pollutants, parasites, and pathogens, appropriate sludge stabilization methods must be applied. However, this method is economical.

2. Recovery from sludge and leachates: Some phosphorus precipitation techniques like struvite and hydroxyapatite may be applied. Investment costs of this method are high. However, the risk of releasing hazardous pollutants and heavy metals is low.

3. Recovery from sludge ashes: To apply this method, some sludge handling methods such as incineration, acidic extraction, and thermochemical treatment should be applied. Therefore, high investment costs are needed. If there is a large amount of excess sludge, this method can be cost-effective (Cieślik and Konieczka, 2017).

Phosphorus can be recovered from the various locations in the wastewater treatment plants (Figure 3.1). The type and the amounts of phosphorus are different depending on the location; therefore, recovery efficiencies will be different at each point.

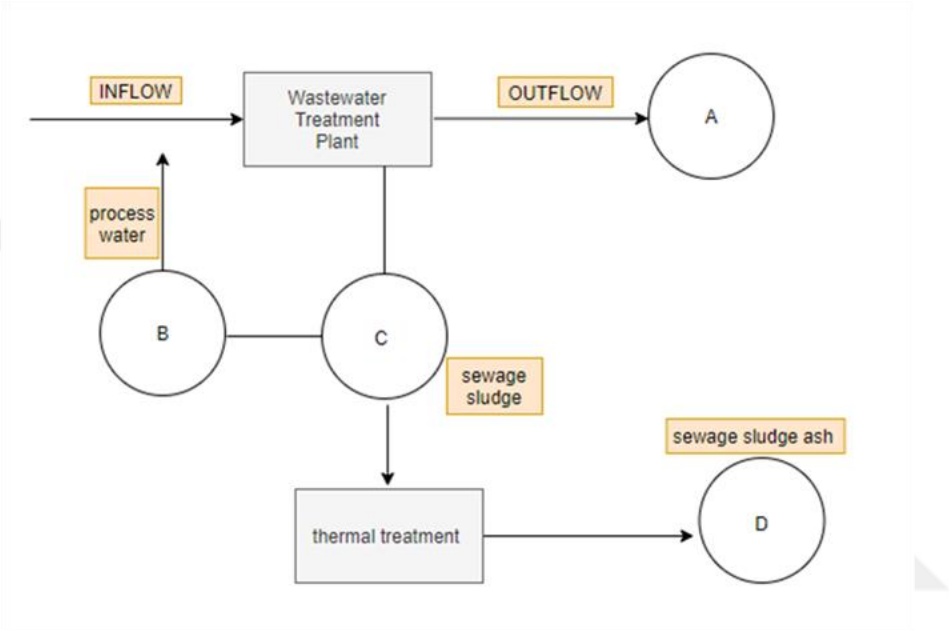

Figure 3.1 Locations for phosphorus recovery in WWTPs (Schönberg et al., 2018)

The potential P recovery amount is between 5 % and 50 % in B point. Theoretically, the high P recovery potential can be achieved in the points C and D (Schönberg et al., 2018).

3.2 Crystallization Process and Chemical Precipitation

Magnesium or calcium salts can be used for the precipitation or crystallization of P. The obtained phosphates (magnesium or calcium ammonium phosphate) can be used as a good plant-available fertilizer after further treatment (Schönberg et al., 2018).

Because of its relative simplicity, struvite (MAP) precipitation is the most widely used P recovery method commercially.

By adding magnesium in the form of soluble $MgCl_2$ to liquid phase containing high phosphorus to achieve appropriate Mg:P ratio, magnesium ammonium phosphate (struvite) occurs. The pH is adjusted as 8–9 using NaOH, at which point struvite crystals start to form. It has a high recovery potential of up to 90%. However only up to 40% of the P can be recovered by this method; the remaining 60% is lost to the sludge. Struvite is used as a slow-release fertilizer, but its large-scale applications are limited despite increased production (Jupp et al., 2021).

3.2.1 MAP Crystallization

MAP is commonly known as struvite. Struvite crystallization is a method for removing phosphorus and reusing it. MAP can be used as a phosphate fertilizer in crops. It is a white-colored powder that oblique rectangular crystal (Cheng et al., 2017). Structure of MAP and characteristics of MAP are given in Figure 3.2 and Table 3.1, respectively.

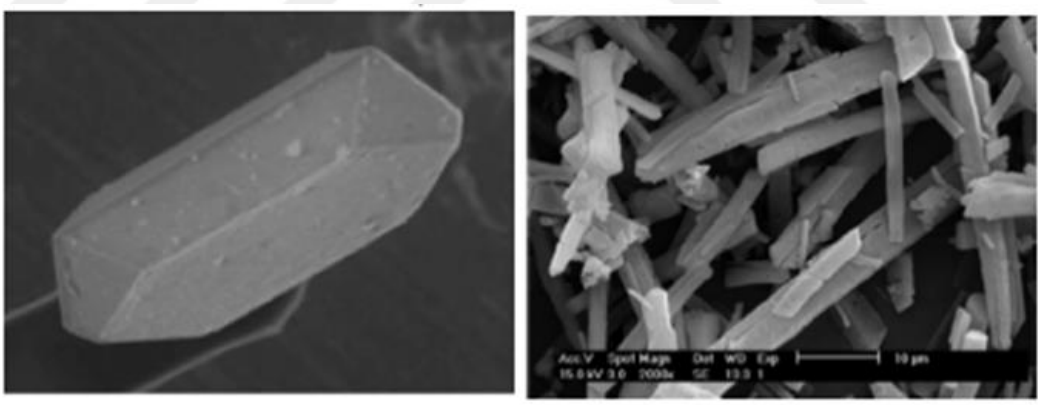

Figure 3.2 Structure of MAP crystals (Corre et al., 2009)

Table 3.1 MAP characteristics

Chemical Formula	$MgNH_4PO_4.6H_2O$
Molecular weight	245.43 $g.mol^{-1}$
Specific gravity	1.711 $g.cm^{-3}$
Solubility constant	$10^{-13.26}$

MAP crystallization is a hard process and there are multiple factors that affect crystallization. These factors are pH, supersaturation level, common ion effect, and mixing speed (Cheng et al., 2017). Better crystallization performance will let the better removal rate and phosphorus recovery. That's why it's important to meet the required crystallization parameters. Magnesium phosphate crystallization reactions are shown below (Cheng et al., 2017):

$$NH^{+4}+H_2PO^{-}_4+Mg^{+2}+6H_2O \leftrightarrow MgNH_4PO_4{\cdot}6H_2O+2H^{+}$$

$$NH^{+4}+HPO^{-2}_4+Mg^{+2}+6H_2O \leftrightarrow MgNH_4PO_4{\cdot}6H_2O+H^{+}$$

$$NH^{+4}+PO^{-3}_4+Mg^{+2}+6H_2O \leftrightarrow MgNH_4PO_4{\cdot}6H_2O \quad (3.1)$$

3.2.2 HAP Crystallization

The HAP crystallization is another method that can be used for phosphorus recovery. Since it helps to reduce or eliminate the eutrophication and to recover the mineral resources, it is an environmentally friendly application (Dai et al., 2017).

HAP is known as hydroxyapatite. To obtain hydroxyapatite $PO^{+3}_{4,}$ Ca^{+2} and OH^{-} ions are used (Cheng et al., 2017). The chemical reaction is given below. Unlike MAP, which is formed directly, HAP requires recrystallisation of a precursor phase (Yin et al., 2019).

$$10Ca^{+2}+6PO^{+3}_4+2OH^{-} \rightarrow Ca_{10}(PO_4)^{6+}(OH)_2\downarrow \quad (3.2)$$

3.2.3 Vivianite Crystallization

Phosphorus recovery has been studied with different forms such as Magnesium ammonium phosphate (MAP), hydroxyapatite (HAP), and calcium phosphate (CaP) at pilot or full scales (Corre et al., 2009).

However, studies related to phosphorus recovery as vivianite crystals are rare (Liu et al., 2018). Vivianite and vivianite crystallization will be discussed in detail in other chapters of the thesis.

3.3 Wet Chemical Process

In the wet chemical process, acids are used to reduce pH and converting chemically or biologically bounded phosphorus into dissolved phosphorus. Sulphuric acid, hydrochloric acid, phosphoric acid, or CO_2 are used as an acid source. The degree of dissolution depends on the pH value and thus on the acids used. After releasing of phosphorus different techniques such as precipitation and crystallization are used to separation.

Figure 3.3 summarizes the procedure for wet chemical process. A good plant-available fertilizer can be obtained with this process. Process efficiency and the quality of the products may change depending on the technical and economic effort. Up to 90% recovery efficiency can be achieved from sewage sludge ash (Schönberg et al., 2018).

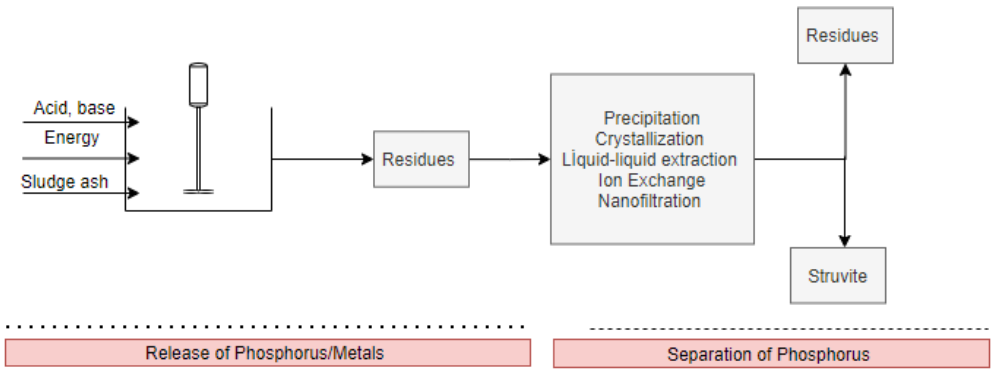

Figure 3.3 Schematic representation of wet chemical process (Cornel and Schaum, 2009)

3.4 Thermochemical Treatment

Thermochemical treatment can be applied to sewage sludge and sludge ashes. Phosphorus containing material, such as sludge or ash, is heated up to 500-1000 ℃. By this application, organic compounds are destroyed and removed via a gas stream. Mineral salts such as chlorides, sulfides are usually added to the process. After addition, heavy metal chlorides can be separated via the gas phase. Recovery efficiency can be reached up to 90% with thermochemical treatment. As a side effect of this process, important ingredients for fertilizer (nitrogen and sulfur) are escaped. It affects the fertilizer quality (Schönberg et al., 2018).

Apart from all these processes, metallurgical processes, ion exchange process, magnetic separator process, forward osmosis membrane distillation, thermal pressure hydrolysis can be used. The potential of phosphorus recovery increases from wastewater through sewage sludge ash path. However, plant availability is an important factor for desired recovery rates (Schönberg et al., 2018).

CHAPTER 4
PHOSPHORUS RECOVERY AS VIVIANITE MINERAL

4.1 Introduction to Vivianite

Increasing the recovery percentage of phosphorus and meeting discharge standards are related to the efficiency of the method used. For this reason, researchers are continuing for the most efficient recovery of phosphorus from wastewater. Recently, the phosphorus mineral called vivianite has attracted a lot of attention.

Vivianite, which is an iron-phosphate mineral ($Fe_3[PO_4]_2.8H_2O$), is named in honor of John Henry Vivian (1785 - 1855), an English mineralogist and mine owner who first discovered this mineral in Cornwall. Pure, fresh vivianite is colorless but oxidizes very easily and changes color from deep blue to black. Physical properties of vivianite are shown in Table 4.1

Table 4.1 Physical properties of vivianite (https://www.mindat.org/min-4194.html)

Formula	$Fe^{2+}_3(PO_4)_2 \cdot 8H_2O$
Colour	Colourless and transparent when fresh, quickly turning pale to deep blue, greenish-blue or bluish-green.
Hardness	1.5-2
Specific gravity	2.67-2.69 g/cm^3
Crystal System	Monoclinic

It is formed in the presence of dissolved ferrous ions and phosphorous in the absence of oxygen. To formation of vivianite, sulfide concentrations must be relatively low in the environment (Pathak, 2019).

4.2 Use of Vivianite as Product

Vivianite stands out not only with its high phosphorus recycling potential, but also with its usage areas in industries such as agricultural, chemical and electronics. Although researches are continuing about the production and conditions of vivianite mineral, the potentials for its use should not be ignored. It can be used as a pigment in painting, a valuable gemstone, source of manufacturing lithium-iron secondary batteries and fertilizer.

Since vivianite is a mineral, rich in phosphorus, its use as a fertilizer has been evaluated. Fodoué et al. (2015) investigated the fertilizing effect of vivianite and found that vivianite (on the Hangloa location) can be used as natural phosphate fertilizer alternative to chemical fertilizers commonly used. Fertilizer yield of vivianite is equal to other forms of recovered P such as struvite and hydroxyapatite. Vivianite can be uptaken by plants more than four to six times than calcium phosphate. It can be used as a slow-release fertilizer (Wu et al., 2019).

Vivianite is also used in the manufacture of lithium iron phosphate ($LiFePO_4$), which is increasingly exploited as a precursor when fabricating Li-ion secondary batteries (Wu et al., 2021).

Vivianite is used as a natural pigment for painting purpose. It is rare and valuable pigment for carpet painting (Janson, 2021)

4.3 Structure of Vivianite

Vivianite is a combination of iron (33.5%), phosphorus (12.3%), hydrogen (3.2 %), and oxygen (51%) [$Fe_3(PO_4)_2 \cdot 8H_2O$]. Vivianite is a blue-green or blue-gray crystal (Antoniewicz, 2018). Structure of vivianite is shown in Figure 4.1.

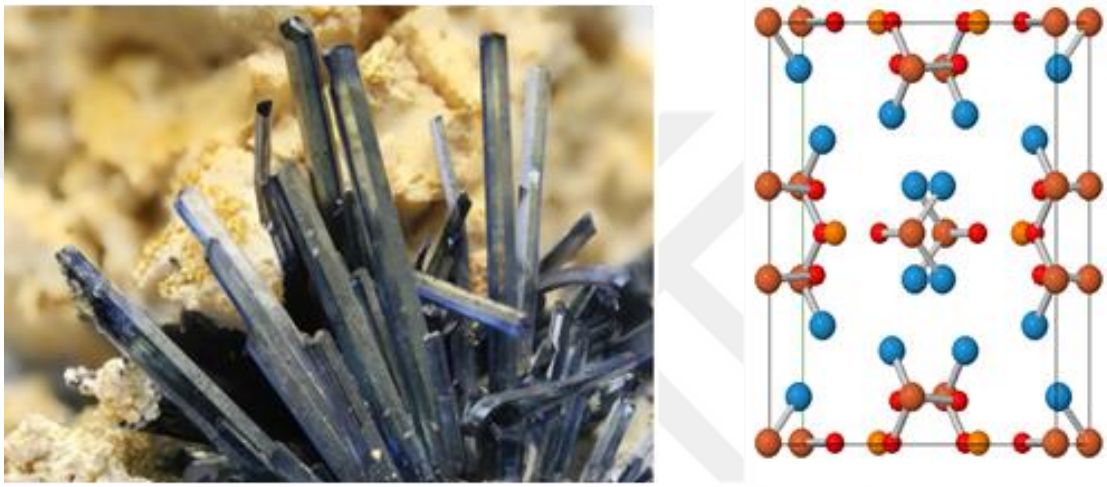

Figure 4.1 Photo and structure of vivianite crystal (https://www.mindat.org/min-4194.html)

Iron and phosphorus are essential to obtain vivianite. Iron dosing helps to flocculation of phosphate. Iron is both found in wastewater and can be dosed. Phosphorus is abundant in wastewater in three two forms organic phosphorus, inorganic phosphorus, and polyphosphates.

Dissimilatory metal-reducing bacteria (DMRB) decrease iron ion (Fe^{+3}) to (Fe^{+2}) whereas anaerobic microorganisms change organic phosphorus to phosphate. As these two microbial processes proceed, a local habitat is created where Fe^{+2} and PO^{-3}_4 concentrations rise. Vivianite would form once the solubility product (K_{sp}) value reached the required requirement. The corresponding chemical reactions are displayed below (Wu et al., 2019).

$$\text{Organic Phosphorus} \longrightarrow PO^{-3}_4$$

$$Fe(OH)_3 + 3H^+ + e^- \longrightarrow Fe^{+2} + 3H_2O$$

$$3\,Fe^{+2} + 2PO^{-3}_3 + 8H_2O \longrightarrow Fe_3(PO_4)_2.8H_2O \quad (4.1)$$

Microorganisms are an important factor in both the recovery of phosphorus and the formation of vivianite. Basically, they play an active role in the mechanisms. First, the reduction of trivalent iron ions to divalent iron ions is carried out by DMRB. Although it is not directly seen in the reactions, the formation of vivianite is affected by the amount of sulfide in the environment. SO_4^{2-} to S^{2-} through the reduction by sulfate-reducing bacteria (SRB) (Wu et al., 2019).

4.4 Vivianite in WWTPs

Vivianite mineral is not only found in wastewater, but also in various aquatic and terrestrial ecosystems, such as freshwater and marine sediments, swamps, hydrothermal deposits, and archaeological environments (Rothe et al., 2016).

Vivianite can be formed different sides of the WWTPs. It is formed when anaerobic digestion releases phosphate and changes ferric iron to ferrous iron, then the ferrous iron precipitates with sulfide and phosphate to form vivianite (Antoniewicz, 2019). It can be occurred thickened sludge pipes due to the reduction of ferric ions. CO_2 stripping occurring during centrifugation of undigested sludge caused a pH increase, responsible for the formation of vivianite. It is visible on the inside of heat exchangers used to heat digested sludge. This is because vivianite's solubility is temperature dependent (Prot et al., 2021).

Table 4.2 shows the compassion between vivianite and struvite. When the struvite and vivianite minerals are compared, it is seen that vivianite is superior. Considering the pH values in which both minerals are formed, it is seen that more alkaline conditions are required for struvite. Wastewater treatment plants generally operate in the neutral pH range. Therefore, it may be necessary to add alkali to aid struvite formation. This is not the case for vivianite.

Vivianite is superior comparing to struvite. Considering the pH values in which both minerals are formed, it is seen that conditions that are more alkaline are required for struvite. Baldan and Filibeli (2008) reported that, the best phosphorus removal was detected at pH 9 and 10. However, wastewater treatment plants generally operate in the neutral pH range. Therefore, it may be necessary to add alkali to aid struvite formation whereas this is not the case for vivianite.

In addition, iron dosing is necessary for vivianite formation, yet it already exists in wastewater itself. Iron has its own specifications in the wastewater such as reducing the emission of hydrogen sulfide compounds, which causes odor problems in wastewater.

Iron can increase the efficiency of anaerobic digestion in terms of parameters including CH_4 production, H_2S control, dewatering ability, volatile solid removal, and pharmaceutical and personal care product (PPCP) degradation. Iron salts are frequently added to wastewater as flocculants to remove P to comply with strict effluent standards (Wu et al., 2019).

When compared to the relatively low percentage (30%-40%) of struvite from wastewater, which is only possible in WWTPs with enhanced biological P removal (EBPR), vivianite recovery efficiency can currently reach 62.1% with lots of room for future improvement. Economically, the market price of vivianite is more expensive than struvite. Vivianite can be more profitable in future applications (Wu et al., 2019).

Table 4.2 Comparison of vivianite and struvite (Wu et al., 2019)

P recovery methods	**Vivianite**	**Struvite**
Chemical equation	$Fe_3(PO_4)_2(H_2O)_8$	$MgNH_4PO_4.6H_2O$
pH	6.0-9.0	8.0-9.5
Extra reagents dosing	Fe salts	Mg salts
Applicable treatment process	Conventional treatment process	EBPR
Recovery efficiency	62% (MBR-with co-fermentation)	30-40%
The value of products	10,000 €/t	500 €/t

4.5 Phosphorus Recovery as Vivianite Mineral

Vivianite has widespread attention for phosphorus recovery. Recently, there are lots of papers about the recovery of phosphorus as vivianite. Both economical value and uses of vivianite have promising future. The market value of vivianite is priced at 10,000 €/ton. Besides this, it's a slow-release fertilizer and source for lithium iron phosphate manufacturing. There are different studies about the recovery efficiency of phosphorus via vivianite minerals. Different techniques have been studied and methods are be examined in feasibility. Magnetic separation, crystallization, and separation by centrifugation are techniques for phosphorus recovery as vivianite (Wu et al., 2019).

Crystallization is one of the techniques used to recover vivianite. Simple design, easy application, efficient recovery, and low environmental risks make this method ideal. A fluidized bed reactor is the most common method for crystallization process. The reactor is filled with seed material and the crystallization reaction occurs on this material. However, it is not easy to detect vivianite and observe the formation and growth of vivianite crystals (Wu et al., 2019).

4.5.1 Magnetic Separation

Vivianite's magnetic properties distinguish it from other phosphorus minerals. The only major mineral in the sludge that exhibits paramagnetic activity is vivianite. It is separated by magnetic separation with the aid of this paramagnetic specialty (Prot et al., 2019).

Lab-scale studies belonging to Prot et al. showed that the separated fractions consist of 52–62% of vivianite, 20% of organic matter, less than 10% of quartz, and a small quantity of siderite. This method has been found promising and it can be developed for large-scale applications (Prot et al., 2019).

There is a project called “ViviMag” based on magnetic separation of vivianite by Wetsus. It’s basically a large-scale application of vivianite separation based on magnetic separation (https://www.wetsus.nl/european-projects/vivimag).

4.5.2 Crystallization

Vivianite minerals are formed through a process called crystallization that relies on solution supersaturation. It is a simple application process. However, conditions including ambient temperature, solution supersaturation, ionic strength, and pH limit the synthesis of vivianite in the solution system (Wu et al., 2021).

Fluidized bed crystallization is used for obtaining vivianite. The reactor is filled with seed material as a carrier. It’s important to provide accurate supersaturation for crystal formation. Wu et al., obtained 95% phosphorus removal and 63% crystallization ratio with fluidized bed crystallization reactor using TFT-LCD manufacturing wastewater (Wu et al., 2019). There are different studies based on fluidized bed crystallization of vivianite and batch experiments.

Crystallization is a promising technique and when process parameters are optimized and controlled during crystallization better results can be achieved.

4.5.3 Centrifugation

Centrifugation is another method used for separating vivianite from sludge via density difference. Densities of vivianite mineral and sludge are 2.68 g/cm^3 and 1.0 g/cm^3, respectively (Wu et al., 2019).

In literature, Rothe et al. observed dark blue vivianite nodules in the high-density samples. These nodules are not appeared below the 2.3 g/cm^3 using a reflected light microscope (Rothe et al., 2015).

CHAPTER 5
CRYSTALIZATION

5.1 What is Crystallization?

Crystallization refers to the formation of solid crystals from a homogeneous solution. Supersaturation occurs when the solvent of a solution contains more solid that can ordinarily be accommodated at that temperature (Reciprocal Net., 2004).

Atoms, ions, or molecules are organized into rigid crystals during the crystallization process from gas, melt, or most frequently from solution. In industry, crystallization is a common separation and purification method. Essentially, there are three steps to crystallization. A supersaturated solution is necessary. It is possible for nucleation to occur in supersaturated solutions. Usually, a few seed crystals are required to start the nucleation process. Crystals start to form when stable nuclei are generated. Because the substance's particles are connected to the crystals when crystals form, the concentration of the solution decreases. The crystal growth may continue until the solution reaches its saturation threshold. The solution is then no longer oversaturated. The crystal development typically stops before the saturation point is reached (South-Eastern Finland University of Applied Sciences, 2021).

The classification of nucleation mechanisms is shown in Figure 5.1. Supersaturation is a crucial factor to begin crystallization (Binev, 2015). However, it is not enough just itself. Before crystal growth, there must be nuclei or seeds that act as the center of crystallization. Different nucleation mechanisms can be seen in crystallization operations.

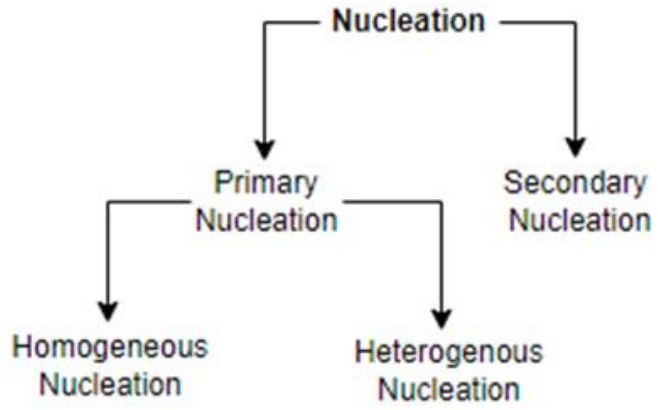

Figure 5.1 The classification of nucleation mechanisms (Binev, 2015)

5.1.1 Nucleation

Primary nucleation occurs in the solution that doesn't contain any crystal body before starting the crystallization. In other words, nucleation doesn't affect the existence of other solid phases (Atalay, 2006).

- Homogeneous Nucleation: Homogeneous nucleation is the process of nucleation that takes place away from the surface of the system. It is a slower process than the heterogeneous type of nucleation. Therefore, this is less common (Madhu, 2018).
- Heterogeneous Nucleation: Heterogeneous nucleation is the nucleation process that occurs at the system's surface. It moves along more quickly than homogeneous type nucleation. Further, this type of nucleation occurs at nucleation sites, an interface between liquid and vapor. Suspended particles, bubbles, the surface of the solution might act as a nucleation site. This type of nucleation occurs more frequently than the homogenous types (Madhu, 2018).

For the formation of nuclei, the energy barrier must first be overcome. This energy barrier is expressed by the change in Gibbs free energy (Atalay, 2006).

The free energy barrier is higher for homogeneous nucleation than heterogeneous nucleation (Madhu, 2018).

Secondary nucleation can be defined as occurring new nuclei from crystals that occurred and grown previously in the supersaturated solution (Atalay, 2006).

5.1.2 Crystal Growth

Following nucleation, crystal embryos expand in size until they form visible crystals. This process is known as crystal growth. The main factors influencing growth rate are mechanisms for surface integration and mass transfer. Although nucleation appears to be the most crucial stage in the formation of struvite crystals, mechanisms involved in crystal growth cannot be overlooked because they are in charge of the crystals' final size and structure (Corre et al., 2009).

Induction time can be expressed as the sum of crystal nucleation time and crystal growth time. Experimentally induction time can be detected by using different analyses such as turbidity, conductivity, absorbance measurements, or pH measurements. Induction time is mainly affected by the supersaturation level (Corre et al., 2009).

5.2 Fluidized Bed Crystallization

Fluidized bed crystallization is a process, where a solution is circulated through a crystallizer in which seed crystals are suspended by the up-flowing fluid. It can be batch or continuous. Fluidization is a technique that has superiorities as regards other techniques. Good solids mixing, the uniform temperature inside the reactor, high mass and heat transfer, and easy solids handling can be shown as examples of these superiorities (Binev, 2015).

A fluidized bed reactor is generally a cylindrical shape reactor that is filled with seed material such as silica, sand, etc. The operation of fluidized bed reactor is shown in Figure 5.2. Crystals have occurred on the seed material via supersaturation. The direction of the flow is upward direction, seed materials are getting bigger shape according to retention time. When particles are big enough, they are settled by gravity, and they can be discharged at the bottom of the reactor.

Fluoride removal, arsenic removal, phosphate removal, heavy metal removal, and water softening operations can be shown applications of fluidized bed crystallization in the industry. By this method, sludge formation is less than conventional precipitation operations (Industrial Technology Research Institute., nd).

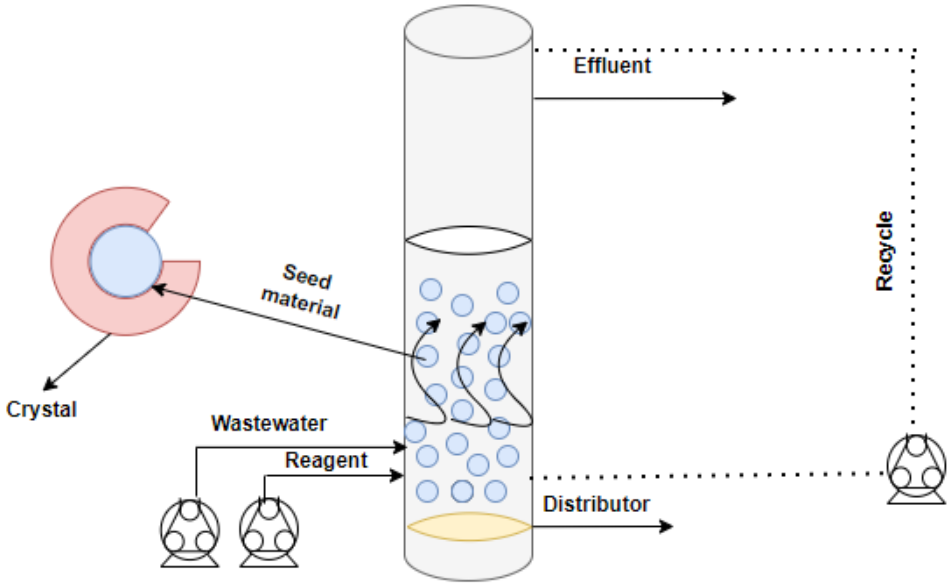

Figure 5.2 Operation of fluidized bed crystallization (Industrial Technology Research Institute)

Liquid-solid fluidized bed reactors can be used in different operations of ion exchange, adsorption, crystallization, etc. In wastewater treatment, fluidized bed crystallization is a studied technique for the removal of unwanted bodies from wastewater. Removal of fluoride, lead, or phosphorus can be achieved by this method. When optimum process parameters are provided and the system is supported by different techniques (in case it is necessary for meeting the discharge standards), high removal rates can be achieved (Binev., 2015).

The particles stay immobile as a fluid moves upward through a dense layer of particles at low velocities. According to the Ergun equation, the pressure drop increases as the fluid velocity increases (Eq. 5.1). Upon further increases in velocity, conditions finally occur where the force of the pressure drop times the cross-sectional area just equals the gravitational force on the mass of particles minus the buoyant force of the displaced fluid. The beginning of fluidization, also known as minimal fluidization, occurs when the particles first start to move. (McCabe et al., 1985; Perry et al., 1997; Geankoplis, 2003)

$$\frac{\Delta P}{\Delta L} = \frac{150\mu\vartheta(1-\varepsilon)^2}{\varphi Dp\varepsilon^3} + \frac{1{,}75\rho\vartheta^2(1-\varepsilon)}{\varphi Dp\varepsilon^3} \qquad (5.1)$$

ΔP: Pressure drop, Pa

ΔL: height of the bed, m

μ: fluid viscosity, kg/m.s

ε: void fraction of bed

ρ: density of the fluid, kg/m^3

ϑ: fluid velocity, m/s

Dp: particle diameter, m

Where; ΔP is pressure drop, Pa; L is the height of the bed, m; ν is the velocity of the fluid based on empty bed cross-section, m/s; ε is the porosity, ρ is the density of the fluid, kg/m^3; μ is the viscosity of the fluid, kg/m.s; Dp is the diameter of the particles, m and ϕ is sphericity.

Porosity is the ratio of volume of voids to volume of bed. The form of many particles in bedding is frequently erratic. The diameter of a sphere with the same volume as a particle is its equivalent diameter.

The ratio of the surface area of this sphere with the same volume as the particle to the actual surface area of the particle is known as the sphericity shape factor of a particle.

Sphericity is the measure of how close a material's shape is to a sphere. Table 5.1 shows various materials and their corresponding sphericity values.

Sphericity and porosity at minimum fluidization point are accepted as 0.88 and 0.42 respectively. Shape factors are given versus material type in Table 5.2.

Table 5.1 Shape factor and void fraction (Geankoplis, 2003)

Type of particles	**Particle Size, Dp (mm)**			
	0.06	0.10	0.20	0.40
	Void Fraction, ε_{mf}			
Sharp sand (ϕ_s = 0.67)	0.60	0.58	0.53	0.49
Round sand (ϕ_s = 0.86)	0.53	0.48	0.43	0.42
Anthrachite coal (ϕ_s = 0.63)	0.61	0.60	0.56	0.52

Table 5.2 Shape factor and material relationship (Geankoplis, 2003)

Material	**Shape factor (ϕ_s)**
Spheres	1.00
Cubes	0.81
Cylinders	0.87
D_p=h (length)	
Berl saddles	0.30
Rasching rings	0.30
Coal dust, pulverized	0.73
Sand, average	0.75
Crushed glass	0.65

The relation between bed height L and porosity ε is as follows for a bed having a uniform cross sectional area A. Since the volume LA (1- ε) is equal to the volume of solids if they existed as one piece (Geankoplis, 2003; McCabe et al., 1985).

$$L^1A(1-\varepsilon^1) = L^2A(1-\varepsilon^2) \quad (5.2)$$

Where L^1 is height of the bed with porosity ε^1 and L^2 is height with porosity ε^2.

Type of flow whether turbulent or laminar is determined by Reynolds number (N_{re}). Equation 5.3 shows the formula of Reynolds number.

$$N_{re} = \frac{d\vartheta\rho}{\mu} \quad (5.3)$$

N_{re}= Reynolds Number

d: particle diameter, m

ϑ: fluid velocity, m/s

ρ: density of the fluid, kg/m^3

μ: fluid viscosity, kg/m.s

For small Reynolds numbers, Equation 5.4 is used to calculate minimum fluidization velocity. Where, dp is particle diameter, ρ_p is density of seed material, ρ_f is density of the fluid and ε_{mf} is void fraction at minimum fluidization (Suleiman et al., 2012).

$$V_{mf} = \frac{8(\rho_p - \rho_f)(d_p)^2}{150(1-\varepsilon_{mf})/\varepsilon_{mf}} \quad (5.4)$$

5.3 Batch & Continuous Crystallization

In batch crystallization, homogenous solution is initially filled in the crystallizer. After precipitation ended and pre-determined retention time passed, the solution is discharged. The solution can be separated via proper solid-liquid separation method. Batch processing is more economical for small production capacities of approximately 1 m^3 of product per day or less.

Batch crystallization is easy to operate, and it is possible to clean vessel in every cycle. It helps to avoid product contamination (Lewis et al., 2015).

Compared to batch processing, raw materials and equipment are used more effectively in continuous operation, lowering the cost per unit mass of product. Continuous crystallization is typically used for large capacity and when only one product needs to be processed in each unit. The product quality is more consistent in continuous operation than in batch operation. According to the desired final product, a choice of operating mode can be done (Lewis et al., 2015).

CHAPTER 6
MATERIALS AND METHODS

6.1 Crystallizer Types

In the scope of this thesis both fully mixed (CSTR) crystallizer and fluidized bed (FBR) crystallizer was used. Details of these reactors are given below.

6.1.1 Fully Mixed (CSTR) Type Crystallizer

Experimental studies were first started with a lab-scale batch-operated fully mixed (CSTR) type crystallizer, which was a specially manufactured closed beaker with a volume of one liter (Figure 6.1).

Figure 6.1 Fully mixed crystallizer setup used in experimental studies (Personal archive, 2022)

In the upper part of the system, which is manufactured as a cover, there are a total of five inlets, namely a nitrogen gas inlet and outlet, a thermometer inlet, conductivity and pH probes inlet, and an inlet for iron feeding. Figure 6.2 shows the schematic representation of the inlets at the top of the reactor. There is a separate discharge point to discharge the system from the bottom of the reactor. All the inlets and outlets in the reactor

have been closed by plugging the cork and the system was operated anaerobically by purging N_2 gas. The crystallizer was placed on the magnetic stirrer with digital temperature control. The schematic diagram of the process setup is shown in Figure 6.3.

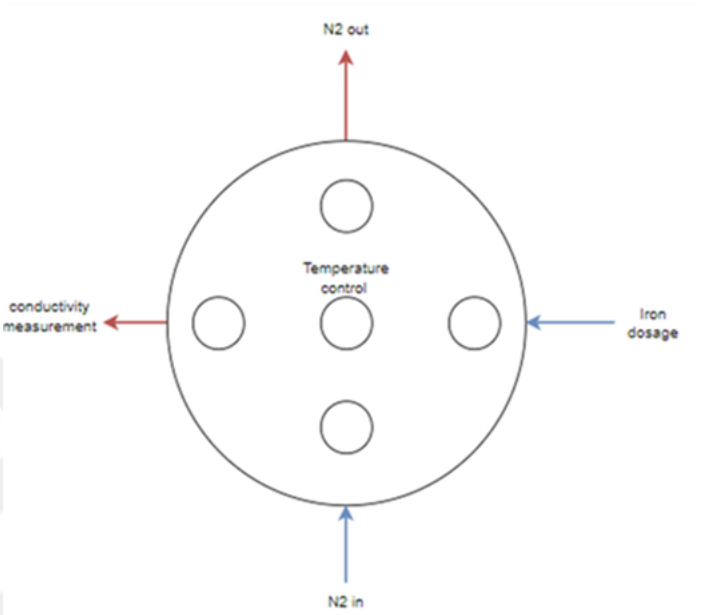

Figure 6.2 CSTR- top view

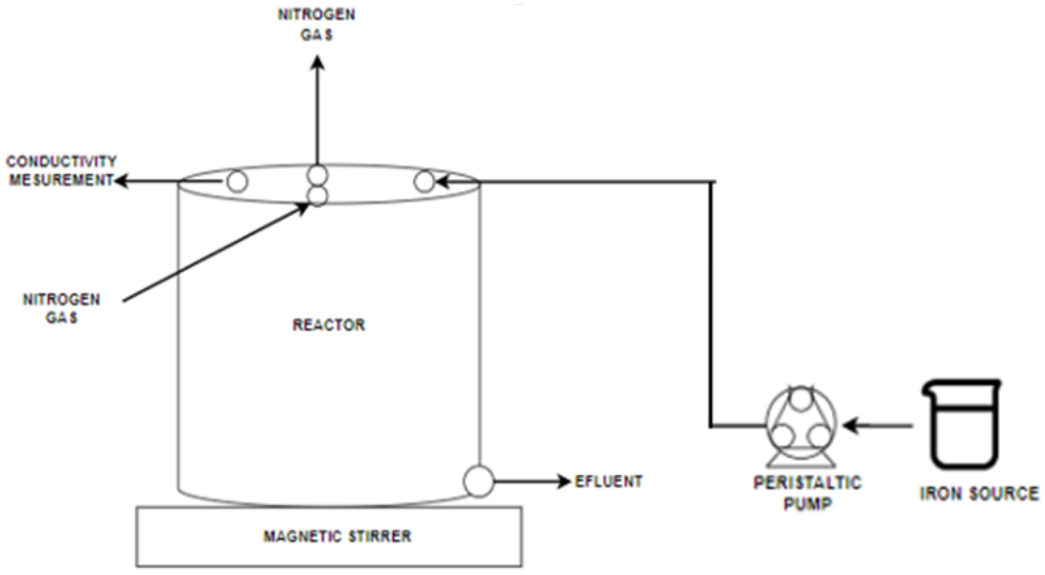

Figure 6.3 Experimental set-up schematic illustration

6.1.2 Fluidized Bed Crystallizer (FBR)

Following experiments with the CSTR system, a fluidized bed crystallizer (FBR) was used. The total height of the reactor is 100 cm. The inner diameter of the reaction zone and settling zone is 3.3 and 6.3 cm, respectively. There are two inlets for phosphorus-containing solution and iron chloride solution. In addition, there is a recycle line from the top of the reactor to the bottom of the reactor. Nitrogen gas was fed to obtain an oxygen-free environment. Experimental set up of fluidized bed reactor and schematic image of the reactor is given in Figure 6.4 and 6.5, respectively.

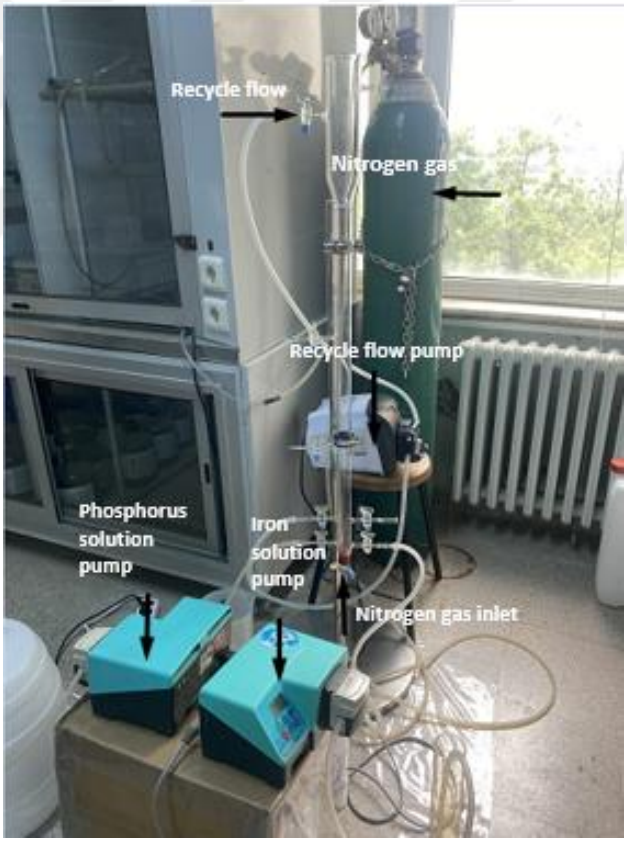

Figure 6.4 Experimental set up of fluidized bed reactor (Personal archive, 2022)

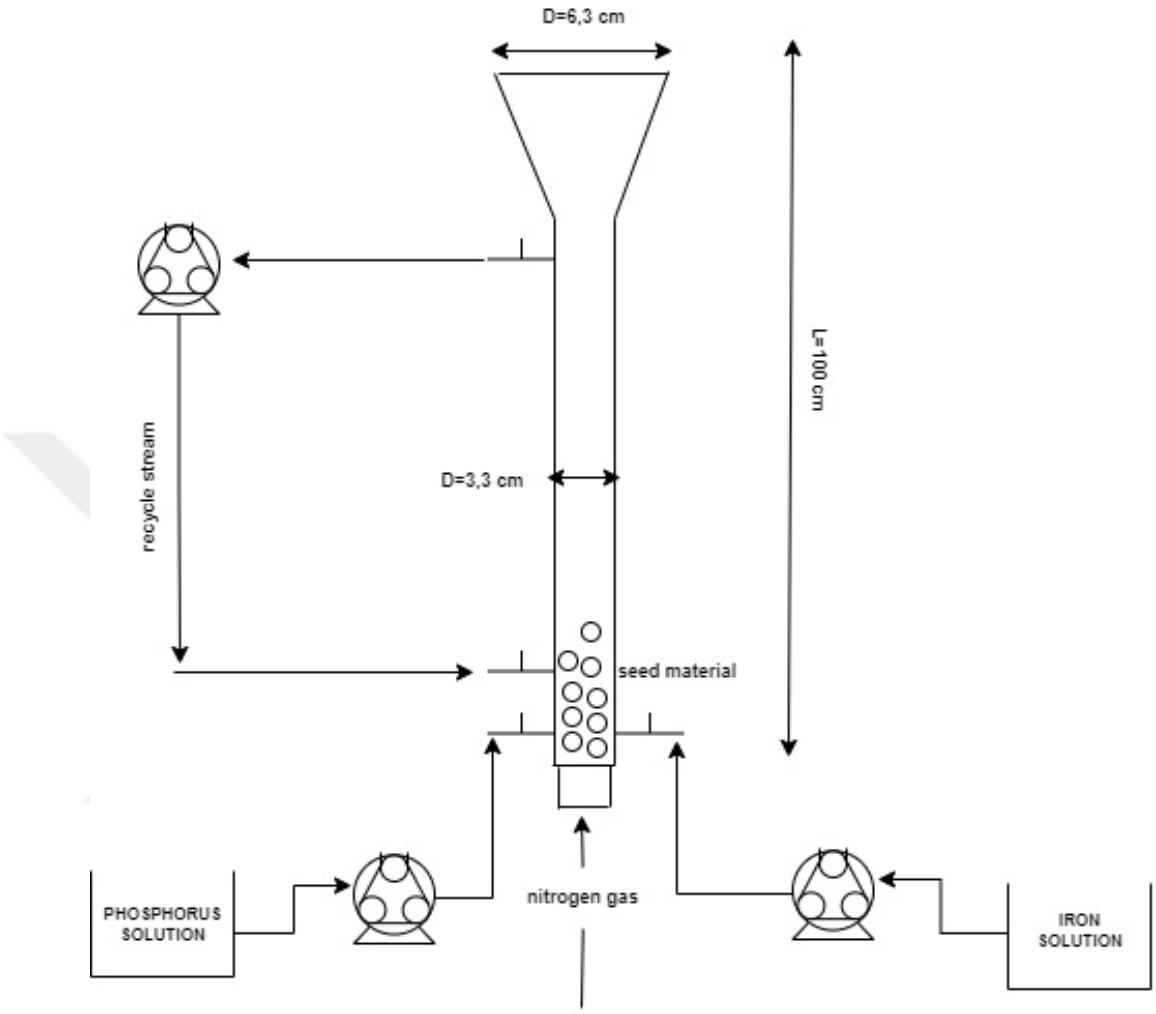

Figure 6.5 Schematic image of fluidized bed reactor

In FBR experiments, ground silica sand was used as a seed material. Original silica sand was ground with a blender before being used in the reactor. The original silica sand and ground silica sand is shown in Figure 6.6. Sieve analyses were done for seed material (ground silica sand) in Civil Engineering Department laboratories of Dokuz Eylul University and the results are shown in Table 6.1. The grain-size distribution graph of the seed material is given in Figure 6.7. The median diameter was found as 0.6 mm (D_{50} = 0.6).

Figure 6.6 Photo of original silica sand (a) and ground silica sand (b)

Table 6.1 Sieve analyses of the seed material

Sieve No	Sieve Opening (mm)	Weight Retained	Cumulative Wt. Retained	% Retained	% Passing
No.4	4.75	0	0	0	100
No.6	3.35	1.42	1.42	0.71	99.29
No.8	2.36	7.36	8.78	4.39	95.61
No.10	2	8.14	16.92	8.46	91.54
No.40	0.425	110.24	127.16	63.58	36.42
No.60	0.25	20.62	147.78	73.89	26.11
No.80	0.18	11.18	158.96	79.48	20.52
No.200	0.076	22.76	181.72	90.86	9.14
Remaining in the sieve		18.28	200	100	0

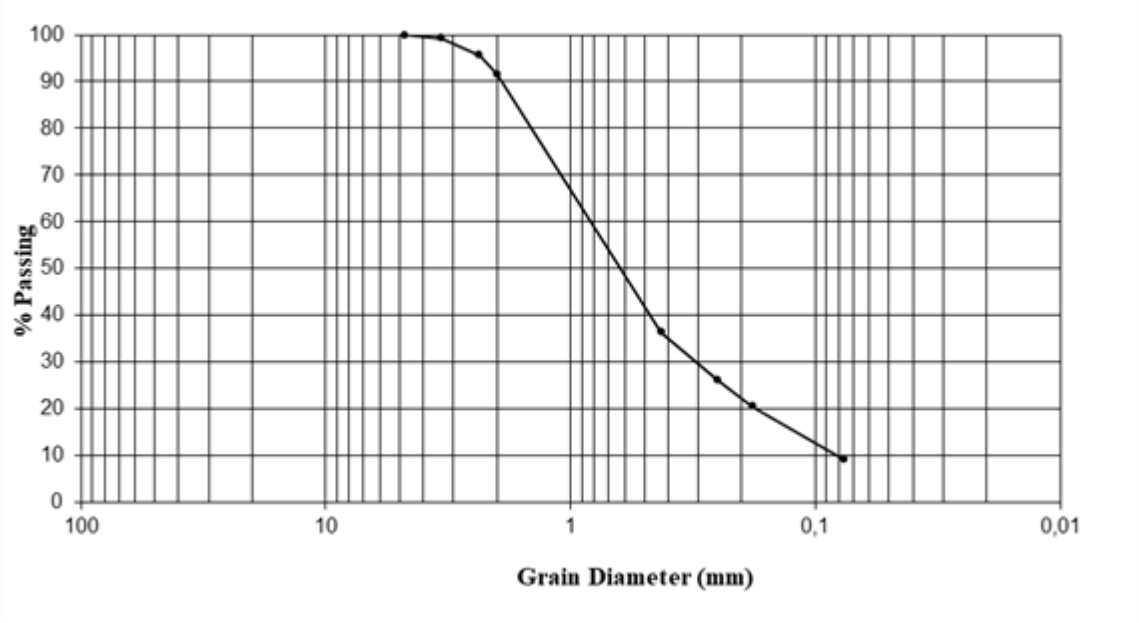

Figure 6.7 Grain diameter distribution graph of the seed material

6.2 Chemicals and Equipment

Sodium phosphate (Carlo Erba 480141) solution and iron chloride (Carlo Erba 451575) solution was used as a phosphorus containing synthetic wastewater and as an iron source, respectively.

WTW Multi 340i Set Portable pH/Conductivity meter was used for monitoring pH and conductivity parameters. Lead Fluid brand YZ15 model medium flow rate pump was used for the recycle stream. Watson-Marlow brand 323Dz model identical pumps were used for water and iron feeds. Phosphate cell test supplied from Merck Millipore (Supelco 1.14729.0001) and filter photometer photoLab® S6 - WTW device was used for phosphorus analyses.

6.3 Operational Conditions

6.3.1 CSTR Crystallizer

Vivianite ($Fe_3(PO_4)2.8H_2O$) has a Fe:P ratio of 1.5:1, stoichiometrically and all solutions were prepared considering this ratio. In all experiments, the initial and final pH values were measured. The pH values of synthetic wastewater prepared with Na_2HPO_4 were around 9.0 ± 0.2. At the beginning of the study, in order to examine the pH effect, the initial pH value was adjusted as 7.0 and 10.0 with the addition of HCl and NaOH, respectively and very little crystal formation occurred at these values compared to the original pH experiments. Therefore, the pH value was not adjusted in subsequent studies. Conductivity monitoring was also carried out to observe the crystal formation and detection of induction time. When the operation of the reactor stops, slower mixing was applied for half an hour and then the sample was settled for 24 hours to perform phosphorus analysis.

The effects of different parameters on vivianite formation were investigated in the experiments performed in the CSTR reactor. These parameters are initial phosphorus concentration, Fe:P ratio, iron feeding rate, iron source, and settling time. At the beginning of the experiments, $FeCl.4H_2O$ and $FeSO_4.8H_2O$ were used as the iron sources and better results were achieved with $FeCl.4H_2O$. Therefore, only $FeCl.4H_2O$ was used in subsequent trials. Parameters and their investigation ranges are shown in Table 6.2. Table 6.3 shows what other process parameters are when examining these parameters.

In the literature, it is stated that the effect of temperature on crystallization is not much (Cheng et al., 2017; Liu et al. 2018). Since the experimental studies were mainly carried out in April-May, the sample temperature was studied between 20-25 °C without any heating process.

Table 6.2 Operating ranges of fully mixed crystallizer

Parameter	**Operational Conditions**
Phosphorus concentration (mg/L)	50 – 100 – 200 – 300 – 400 – 500
Fe:P ratio	1.5:1 - 1.8:1 - 2:1 - 2.2:1 - 2.5:1
Fe feeding rate (rpm - mL/min)	0.5 rpm – 1 mL/min 1 rpm – 3 mL/min 2.5 rpm – 9.4 mL/min 5 rpm – 20 mL/min 10 rpm – 37.5 mL/min 15 rpm – 49,5 mL/min
Magnetic stirrer speed (rpm)	120 (slow mixing) 250 (rapid mixing) / 120 (slow mixing)
Iron Source	$FeCl_2$
Settling time (h)	0.5 – 6 – 7 – 24

Table 6.3 Operating conditions of fully mixed (CSTR) crystallizer

Variable	**Reactor Operating Conditions**	
Initial phosphorus concentration (50-500 ppm)	Fe:P ratio	2
	Fe dosage (rpm)	2.5
	Temperature (℃)	25
	pH	8-9
	Mixing speed (rpm)	250 rpm (5min) + 120 rpm (25min)
Speed of Iron Feeding	Fe:P ratio	2
	Phosphorus concentration (ppm)	100
	Temperature(℃)	25
	pH	8-9
	Mixing speed (rpm)	120
Fe: P ratio	Phosphorus concentration (ppm)	100
	Fe dosage (rpm)	2.5
	Temperature(℃)	25
	pH	8-9
	Mixing speed (rpm)	120
Settling time	Phosphorus concentration (ppm)	100
	Fe:P ratio	2
	Fe dosage (rpm)	2.5
	Temperature(℃)	25
	pH	8-9
	Mixing speed (rpm)	250 rpm (5min) + 120 rpm (25min)

6.3.2 Fluidized Bed Crystallizer

Seed material, which was ground silica sand, was added at a height of 10 cm in the reactor. Phosphorus solution, in which P concentration was 300 mg/L, 400 mg/L, and 500 mg/L, was prepared and then fed to the reactor with the help of a peristaltic pump. At each experiment, P solution was pumped to the reactor, firstly. After the seed materials were completely wet, the iron solution was fed into the reactor by another peristaltic pump. When both flows were given to the system at the same time, mobility began to be observed in the seed materials. When the water level in the reactor reached the height of the recycle flow level, recycle flow was activated with third peristaltic pump. When the iron chloride solution and water feeds to the reactor were complete, recycle flow was the only flow that kept mobility in the reactor. Operation of the reactor ended after ninety minutes.

Three peristaltic pumps were used for operation of the system. Lead Fluid brand YZ15 model medium flow rate pump was used for the recycle stream. Watson-Marlow brand 323Dz model identical pumps were used for water and iron feeds. Recycle stream was operated when reactor liquid level came the pre-determined point. Pumps for phosphorus containing synthetic wastewater, iron solution and recycle were operated at 10, 15, and 20 rpm, respectively.

6.4. Vivianite Formation Analysis

The characterization of the crystals obtained as a result of the experiments was made by SEM, XRD, and SEM-EDS analyses. Vacuum drying with a vacuum oven (Nuve EV 018) was first applied to the obtained aqueous precipitates. The image of the sample after drying is given in Figure 6.8. The samples were then pulverized and made suitable for analysis. With SEM analysis, zoomed images of different sizes of the samples were obtained. It is aimed to observe angular and ordered crystal structures. XRD was used to analyze the obtained crystal material. Vivianite formation was evaluated by comparing the obtained graph and the observed peaks with the literature.

Finally, SEM-EDS analysis was performed. The elemental composition of the samples was investigated by SEM-EDS analysis. The formation of phosphorus and iron in the samples obtained supports the formation of vivianite.

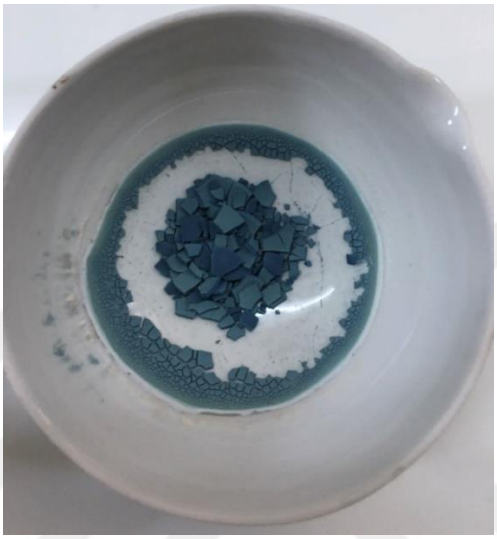

Figure 6.8 The image of the sample after vacuum drying (Personal archive, 2022)

6.5. Particle size distribution

Particle size distribution analysis was carried out in the mixed liquid resulting from the end of the reaction in the experiment, where the best result was obtained in the FB crystallizer. This analysis was performed at Izmir Katip Celebi University. They use a Mastersizer 2000 instrument (Malvern Panalytical, UK). The measurement details are given below:

Dispersant refractive index =1.330

Particle refractive index = 1.569

Laser obscuration = 10.09 %

The average particle size of the vivianite crystal was expresses by d_{50}. This means that particle size corresponding to the percentage of cumulative particle size distribution at 50%.

CHAPTER 7
RESULTS AND DISCUSSION

7.1 Fully Mixed (CSTR) Type Reactor

Phosphorus recovery efficiency was first investigated by using the lab-scale CSTR crystallizer. The pH values of phosphorus solution prepared with Na_2HPO_4 are around 9.0 ± 0.2. In order to examine the pH effect, the initial pH value was adjusted as 7 and 10 with the addition of HCl and NaOH, and very little precipitation occurred at these values compared to the original pH experiments. Therefore, the pH value was not adjusted in subsequent studies. Conductivity was monitored during the experiments.

Four different variables were examined with a set of experiments. These are initial phosphorus concentration of wastewater, Fe:P ratio, speed of iron feeding rate to the reactor and settling time effect on phosphorus removal efficiency. When phosphorus concentration is lower than 50 mg/L, there is no precipitation occurred. The highest phosphorus recovery has been found when Fe:P ratio is 1.8. Maximum recovery efficiency was achieved at speed of iron feeding rate of 10 rpm. Below or above this value phosphorus removal efficiency was lower. For all experiments, phosphorus concentrations were measured after a 24-hour settling time. Below 24 hours settling, the results were considerably lower.

Effects that triggered vivianite formation were investigated and for all trials, parameters that have the highest recovery were highlighted.

7.1.1 Effect of Wastewater P Concentration on Phosphorus Removal via Vivianite Crystallization

The effect of the concentration on the yield was investigated by applying rapid mixing for 5 minutes + slow mixing for 25 minutes + settling for 24 hours. $FeCl_2$ was used as the iron source and $FeCl_2$, which was prepared with a Fe:P ratio of 2, was fed into the reactor at a speed of 2.5 rpm (9.4 mL/min).

Industrial wastewaters may contain various P concentration. Table 7.1 shows the P content of some industrial wastewaters. Moragaspitiya et al. (2019) indicated that, 100–200 mg/L phosphate could be found in supernatant of an anaerobic digestion of waste activated sludge. Considering these values, the P concentration of solutions was adjusted between 50 – 500 mg/L. Yields varying between 42% and 53% were determined in all trials (Figure 7.1). No crystal formation was observed in the experiments, where the phosphorus concentration was below 50 mg/L. Although color change was observed after iron feeding in phosphorus containing solution, no crystal formation was observed. The image of precipitates in 500 mg/L P concentration trials is given in Figure 7.2.

Table 7.1 Phosphorus concentrations in some industrial wastewaters

Wastewater Source	**P, mg/L**	**Reference**
Electro-plating	7.37–12.57	Li et al., 2020
Fertilizer	4528	Gouider et al., 2017
Fertilizer	240	Zhou et al., 2017
Pickling Wastewater from the Steel Industry	300	Zhang et al., 2022
Pharmaceutical	380 (orto-phosphate) 750 (total phosphorus)	Sun et al., 2017

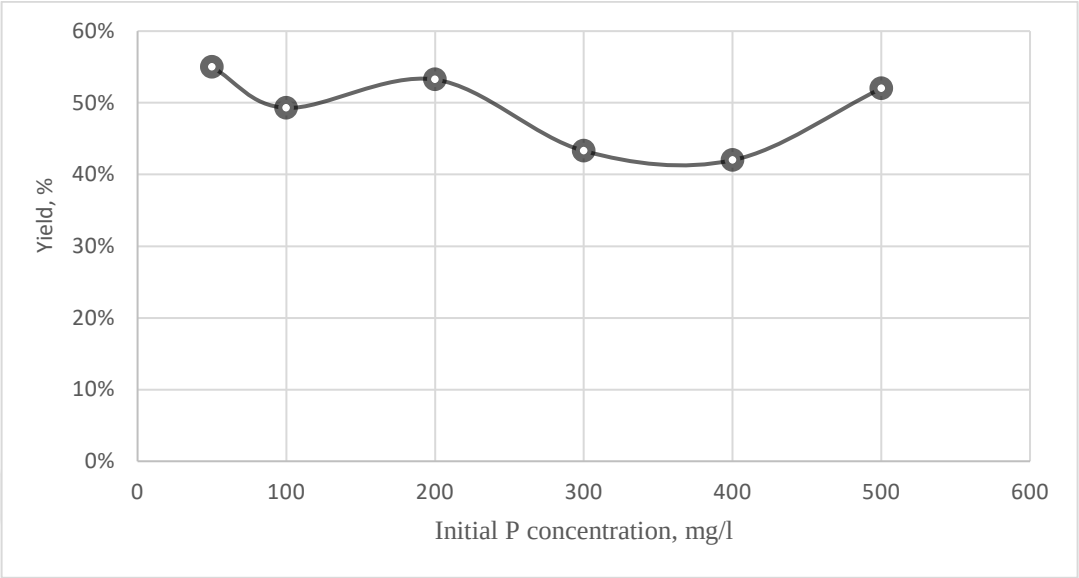

Figure 7.1 Initial phosphorus concentration and phosphorus recovery efficiency

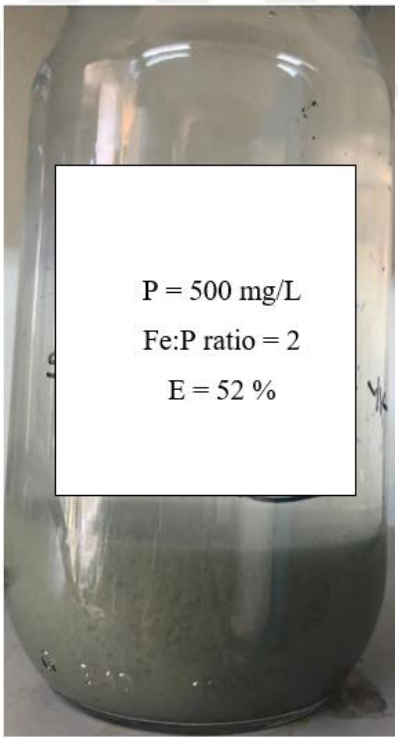

Figure 7.2 Image of precipitates in 500 mg/L P concentration trials (Personal archive, 2022)

7.1.2 The Effect of Iron Feeding Rate on Phosphorus Removal via Vivianite Crystallization

To examine the effect of iron feed rate on P removal efficiency, the $FeCl_2.4H_2O$ feed pump was operated at speeds ranging from 0.5 rpm to 15 rpm. To determine the effect of this parameter, other operating conditions were kept constant. In all trials, reactor mixing speed was taken as 120 rpm, P concentration is 100 mg/L and Fe:P ratio of 2:1. The reaction time varied depending on the iron dosing rate. After the iron dosing was finished, stirring was continued for 5 minutes more slowly and P analyzes were performed after 24 hours of precipitation.

Figure 7.3 shows the relationship between iron dosage and phosphorus removal yield. The highest yield was observed when the iron solution feed at 10 rpm. Below and above this value, yield is lower than 69%. Images of precipitate formed at 15 rpm and 10 rpm feed speed are shown in Figure 7.4.

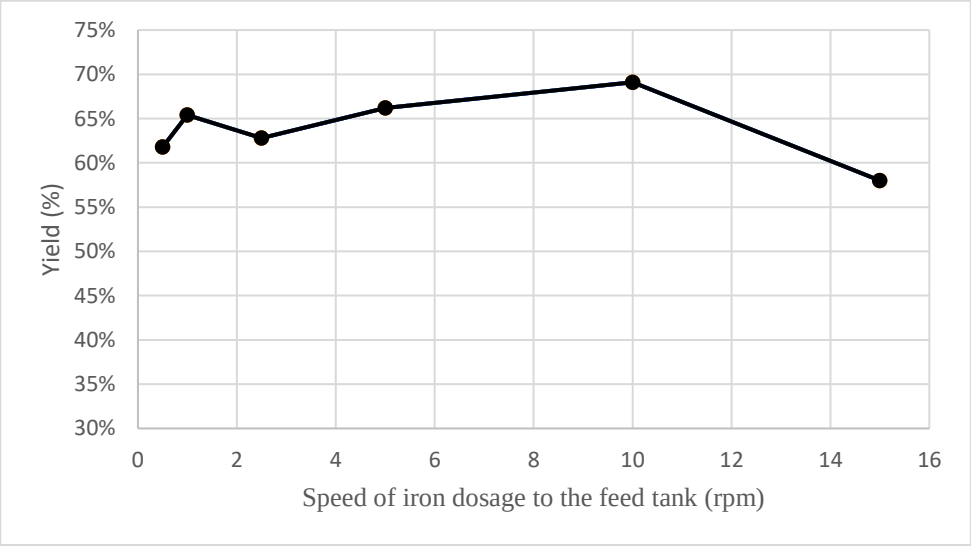

Figure 7.3 Speed of iron dosage and phosphorus recovery efficiency

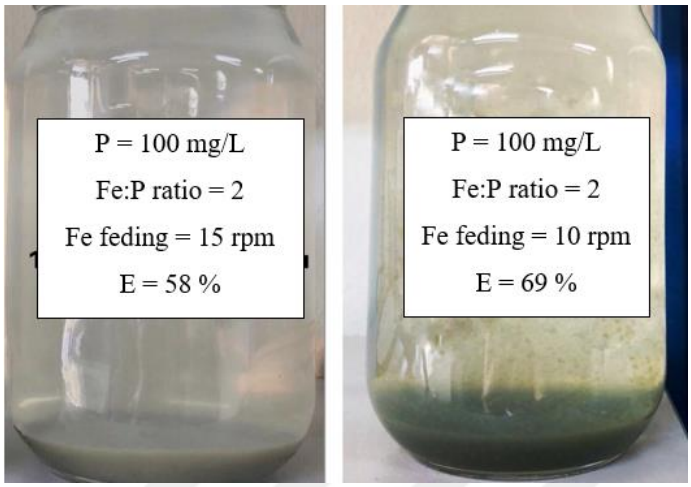

Figure 7.4 Images of precipitate formed at 15 rpm and 10 rpm feed speed (Personal archive, 2022)

7.1.3 The Effect of Fe:P Ratio on Phosphorus Removal via Vivianite Crystallization

The stoichiometric molar ratio of Fe:P in vivianit's chemical formula is 1.5:1. ($Fe_3(PO_4)_2 \cdot 8H_2O$). In literature, experimental studies show that slightly more Fe is required than this ratio to achieve better phosphorus removal (Wu, 2019). With this in mind, phosphorus removal yields were examined for ratios ranging from 1.5:1 to 2.5:1. Figure 7.5 shows the result of Fe:P ratio effect on crystallization. The highest phosphorus removal yield was achieved when Fe:P ratio is 1.8.

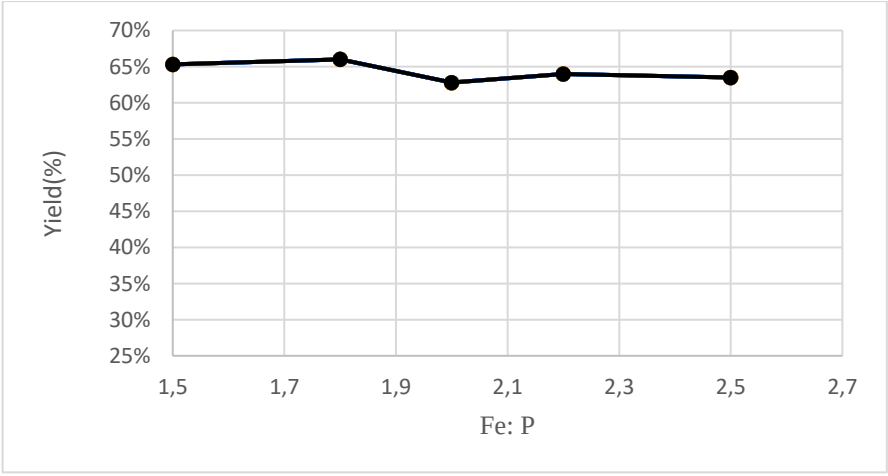

Figure 7.5 Fe:P ratio and phosphorus recovery efficiency

7.1.4 Effect of Settling Time on Phosphorus Removal via Vivianite Crystallization

Priambodo et al. (2017), in their study, applied a 24-hour precipitation process after the reaction time applied in the CSTR system. In this study, there is no explanation as to why 24-hour precipitation was applied. Since 24 hours is a long time, P analyses were carried out at different precipitation times for a series of experiments to investigate whether a shorter period of precipitation could be applied and to decide the time required for the precipitation of the crystals formed after the $FeCl_2$ feed into the phosphorus-containing wastewater was completed. Operating conditions for this experiment were P = 100 mg/L, Fe:P = 2:1, Fe feed rate was set as 2.5 rpm. For the reaction, 5 min rapid mixing + 25 min slow mixing was applied. Figure 7.6 shows that below the 24-hour settling time, the results are significantly lower.

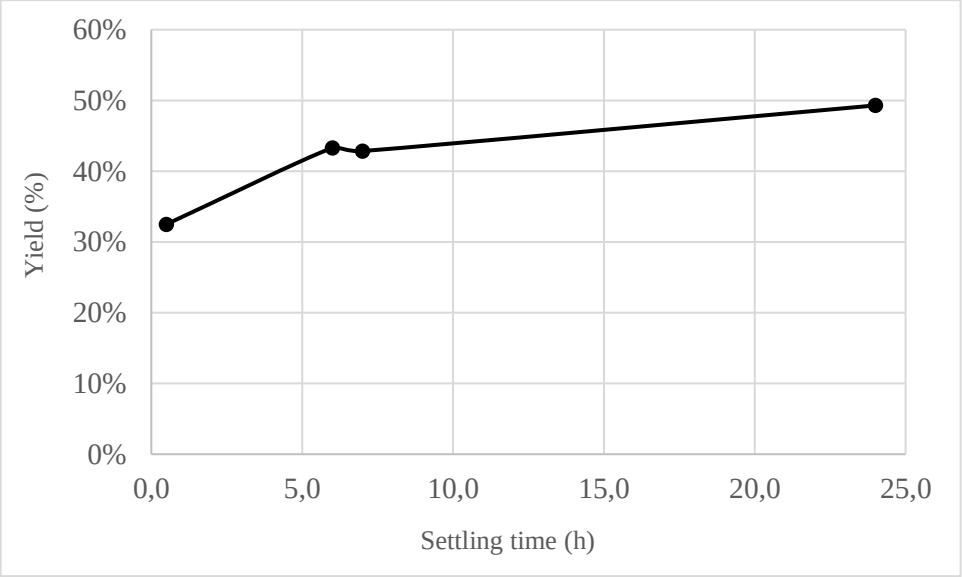

Figure 7.6 Settling time and phosphorus recovery efficiency

7.1.5 SEM Analysis Fully Mixed (CSTR) Type Reactor

Surface morphology of vivianite crystals are determined by scanning electron microscopy. Samples were taken after 24h settling time and dried in Nuve EV 018 vacuum oven. SEM measurements were performed at COXEM EM-30 Plus. SEM images were taken changing between x500 to x10000 magnifications with acceleration voltage of 15-20 kV.SEM images of CSTR reactor type samples are shown in Figure 7.7. In the low magnification, crystals are shown regular and uniform structure. They are close to each other and arranged regularly. Under high magnification levels, sharp corners of crystals are seen.

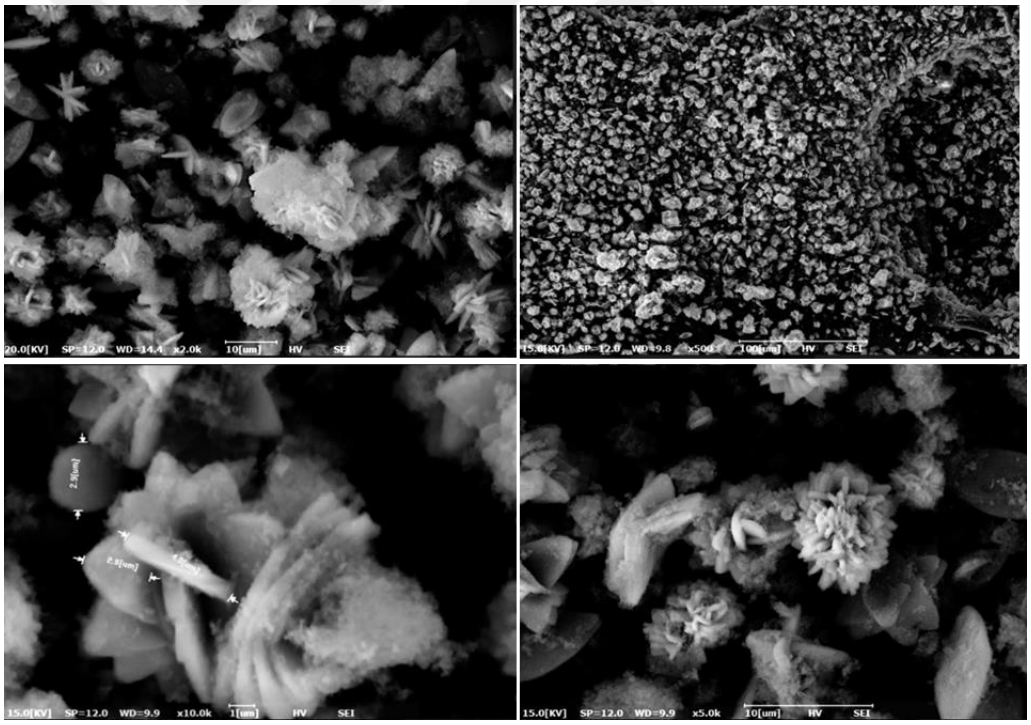

Figure 7.7 SEM images of fully mixed (CSTR) type reactor samples

7.1.6 XRD Analysis Fully Mixed (CSTR) Type Reactor

A diffraction pattern is created by the scattering of X-rays from atoms, and it contains details on the arrangement of the atoms within the crystal. (Banerjee, 2022). Thermo Scientific ARL X'TRA XRD device was used at Dokuz Eylül University Center for Fabrication and Application of Electronic materials. Samples are powdered at 40℃ at vacuum oven for four days at Nuve EV 018 vacuum oven. X-Ray powder diffraction patterns of powder samples are shown in Figure 7.8. To identify whether these X-ray powder diffraction patterns belong to vivianite or not, databases were checked. Peaks at 2θ plane overlapped with vivianite based on the RRUFF™ Database ("Vivianite R070331 - RRUFF Database: Raman, X-ray, Infrared, and Chemistry", 2022). Figure 7.9 shows the vivianite peaks as zoomed in.

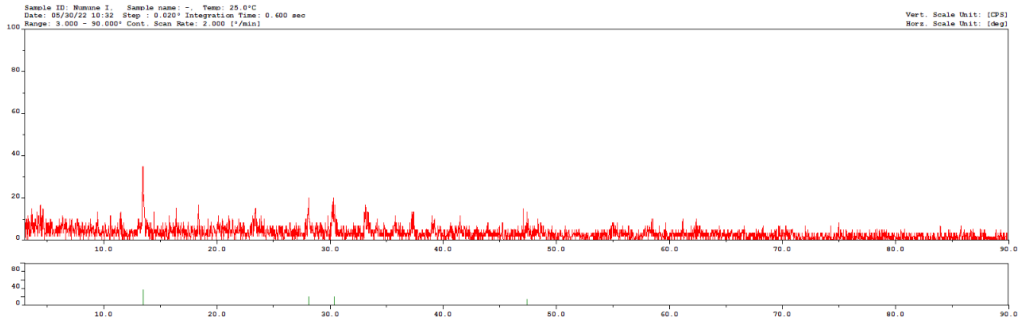

Figure 7.8 X-Ray Diffraction Analysis of Fully Mixed (CSTR) Type Reactor Samples

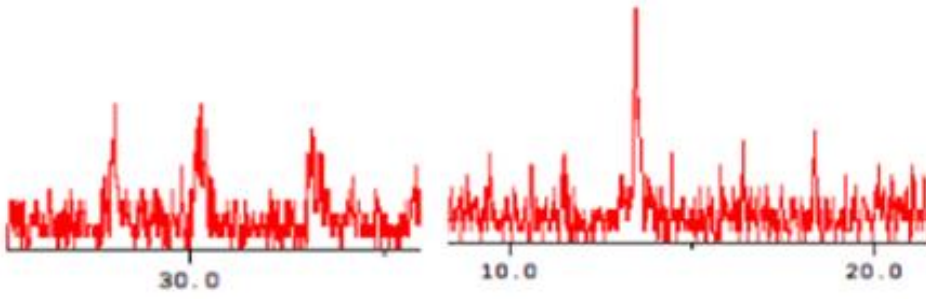

Figure 7.9 X-Ray diffraction analysis of fully mixed (CSTR) type reactor samples (zoom)

7.1.7 SEM-EDS Analysis Fully Mixed (CSTR) Type Reactor

SEM-EDX analyzes were performed at Izmir Katip Celebi University. Carl Zeiss 300VP SEM Device was used and elemental analysis of the sample was made with EDX detector.

The EDS unit has the capacity to identify features within a field of view and collect a spectrum according to various user requirements. The user can focus the X-Ray collection on a single point within a field of view using the point scan. To compare the collected data, multiple point scans may be collected quickly one after the other. The different elemental components found at various sites can then be examined by superimposing these collected spectra onto one another ("Scanning Electron Microscope", 2022).

SEM-EDS analyses were done to determine whether the elemental composition of synthesized material is matched with vivianite or not. The sample, which has the highest phosphorus removal efficiency, was selected for SEM-EDX analysis.

Special regions were determined in the SEM image and the elemental contents of these points were determined as mass and atomic percentage. While interpreting the SEM-EDX results, the chemical formula of vivianite and the Fe:P ratio in this chemical formula were used. Vivianite ($Fe_3(PO_4)_2.8H_2O$) contains iron and phosphorus elements in its structure. The presence of these two elements in the SEM-EDX results is important to confirm the synthesis of vivianite.

When the chemical formula of vivianite is examined, it is seen that the Fe:P ratio is 1.5. From the results obtained from the SEM-EDX results, the ratio of atomic masses of iron and phosphorus elements can be shown as another proof of the existence of vivianite. The closer this ratio is to 1.5, the better the result (Rothe et.al, 2014)

Figure 7.10 shows the SEM-EDS images of CSTR reactor samples. Three selected area and three EDS spot has been determined for analyses. These points were searched for elemental contents. Mass and atomic percentages of each point were given in tables. These mass fractions were evaluated according to their Fe:P ratio. Except selected area 2, phosphorus and iron were determined in all six samples. When Fe:P ratio considered, At EDS Spot 2 and EDS Spot 3, Fe:P atomic mass percentages ratio is 1.6 and 1.5 respectively. These results overlapped with vivianite.

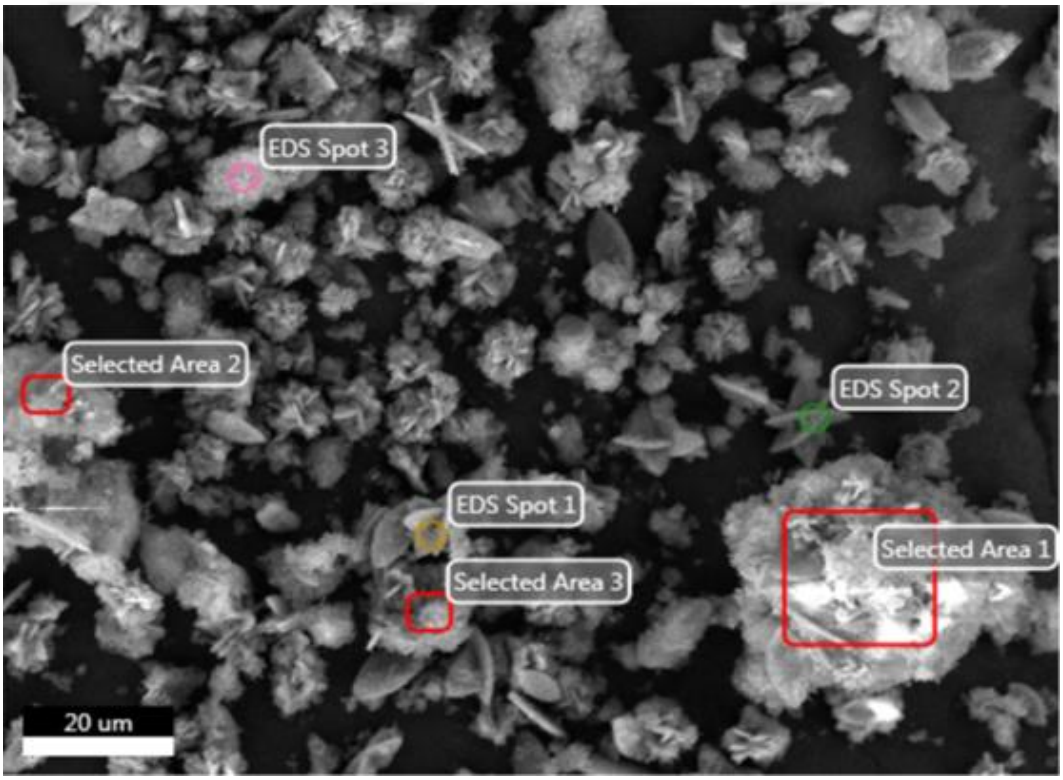

Figure 7.10 SEM-EDS Images of Fully Mixed (CSTR) Type Reactor Samples

Figure 7.11 shows the SEM-EDS graph of selected area 1. The sample contains Fe and P elements, which is essential for characterization of vivianite. In elemental analyses, the element with the highest content is oxygen. Oxygen is undesired element because to obtain vivianite oxygen-free environment should exist. However, while taking samples or during the analyses oxidation can occur. Weight and atomic percentages of the elements in the samples are shown in Table 7.2. Fe:P ratio is 1.28 as an atomic percentage.

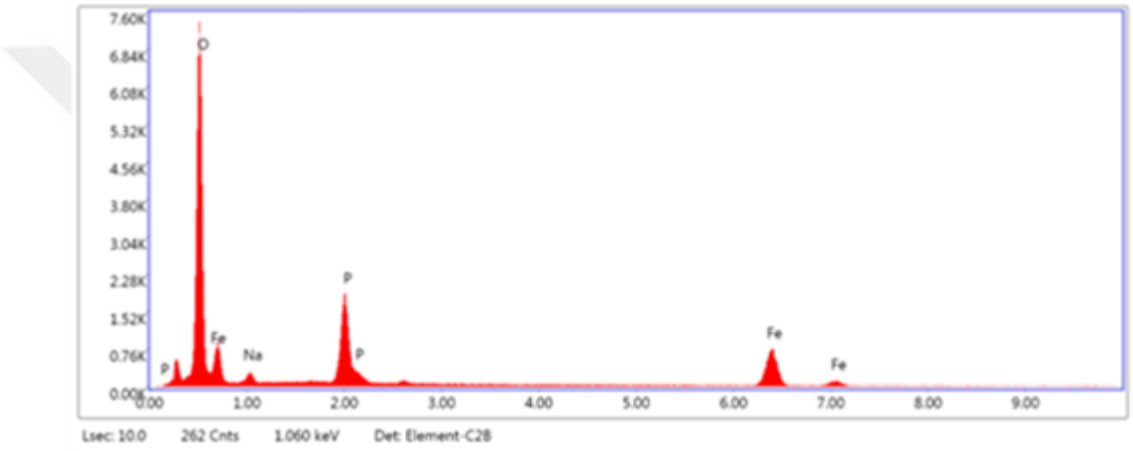

Figure 7.11 SEM-EDX graph of selected area 1

Table 7.2 Elemental analyses of selected area 1

Element	Weight %	Atomic %
O K	44.7	68.18
NaK	2.65	2.84
P K	16.03	12.72
FeK	39.65	16.26

Figure 7.12 shows the SEM-EDX graph of selected area 2. This sample doesn't contain Fe and P (Table 7.3). Only carbon and oxygen elements are detected in this selected area. For tis sample, there is no evidence for vivianite formation.

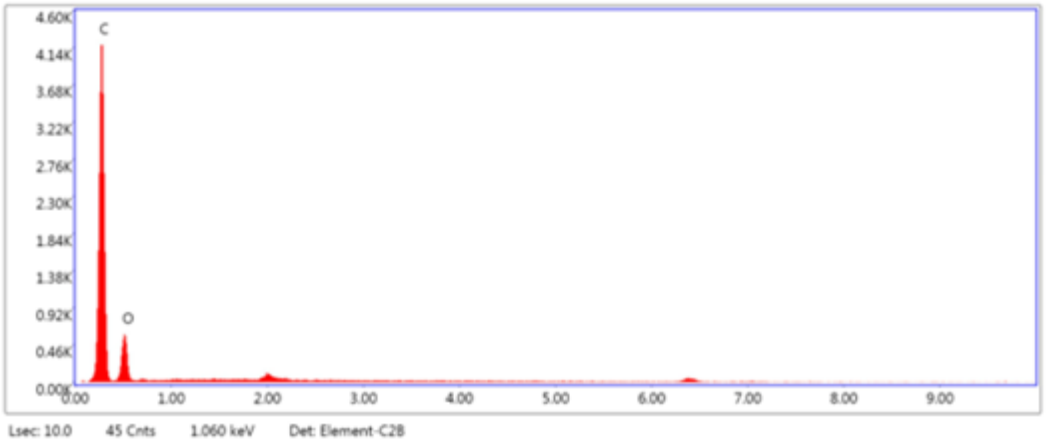

Figure 7.12 SEM-EDX Graph of Selected Area 2

Table 7.3 Elemental analyses of selected area 2

Element	Weight %	Atomic %
C K	74.05	79.17
O K	25.95	20.83

Figure 7.13 shows SEM-EDX results of selected area 3. Oxygen is the element, which has the highest composition in the sample. Fe and P elements involve in this sample. The ratio Fe:P is 1.35 as atomic mass percentage as shown in Table 7.4.

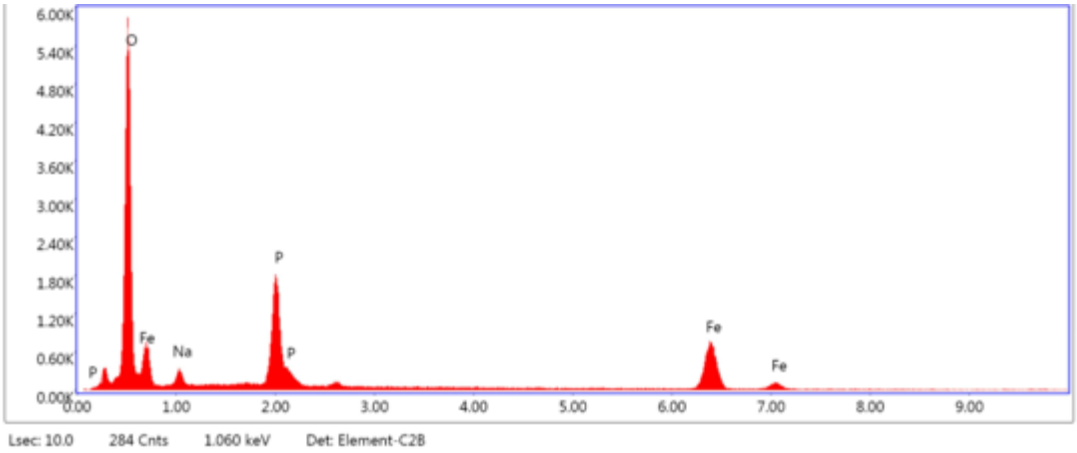

Figure 7.13 SEM-EDX Graph of Selected Area 3

Table 7.4 Elemental analyses of selected area 3

Element	Weight %	Atomic %
O K	38.37	62.35
NaK	4.10	4.64
P K	16.68	14.00
FeK	40.85	19.02

Figure 7.14 shows the SEM-EDX graph of EDS spot 1. In this sample, Fe and P elements involve. This sample is mainly consisting of oxygen and sodium elements. The result of weight and atomic percentages are shown in Table 7.5. Iron and phosphorus are also contained but the percentages are lower than the other elements. The Fe:P ratio is 3.26 as an atomic percentage.

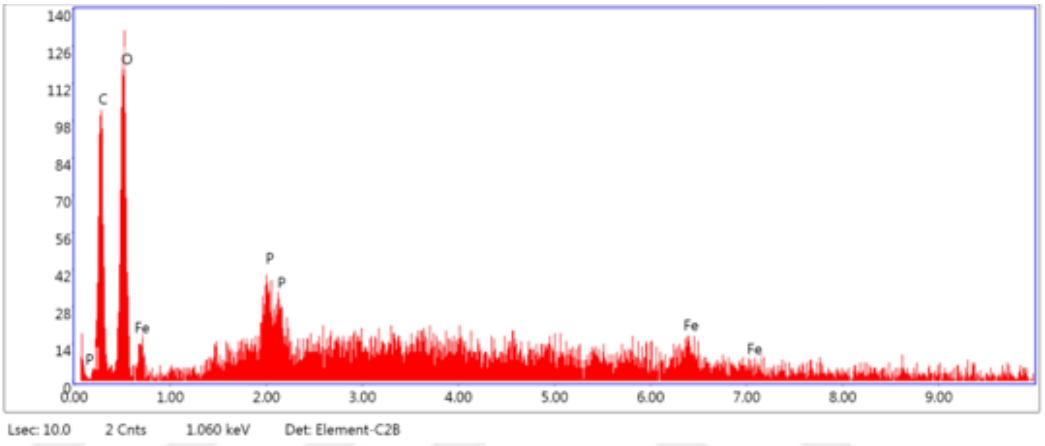

Figure 7.14 SEM-EDX graph of EDS spot 1

Table 7.5 Elemental analyses of EDS spot 1

Element	Weight %	Atomic %
O K	39.56	50.98
NaK	43.48	41.99
P K	6.03	1.67
FeK	10.93	5.45

Figure 7.15 show the SEM-EDX graph of EDS Spot 2. As a weight percentage, iron element has the highest percentage. As an atomic percentage, oxygen has the highest percentage. Oxidation can easily occur. This oxidation can lead to not accurate results. However, the presence of iron and phosphorus elements supports the formation of vivianite. Table 7.5 shows the atomic percentages of the elements in the sample. Fe:P ratio is 1.61.

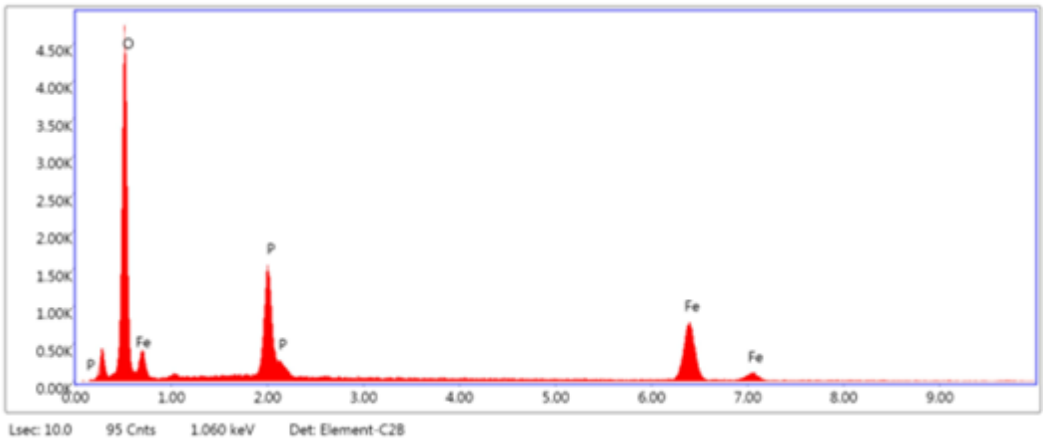

Figure 7.15 SEM-EDX graph of EDS spot 2

Table 7.6 elemental analyses of EDS spot 2

Element	Weight %	Atomic %
O K	35.61	61.56
P K	16.47	14.70
Fe K	47.92	23.73

Figure 7.16 shows the SEM-EDX results of EDS Spot 3. This sample consist of carbon, oxygen, sodium, phosphorus, and iron. When the samples are examined in terms of the presence of vivianite, it is seen that iron and phosphorus contents are present. Table 7.7 shows the mass and atomic percentages of the element contents. As an atomic percentage, it is seen that the Fe:P ratio is 1.54.

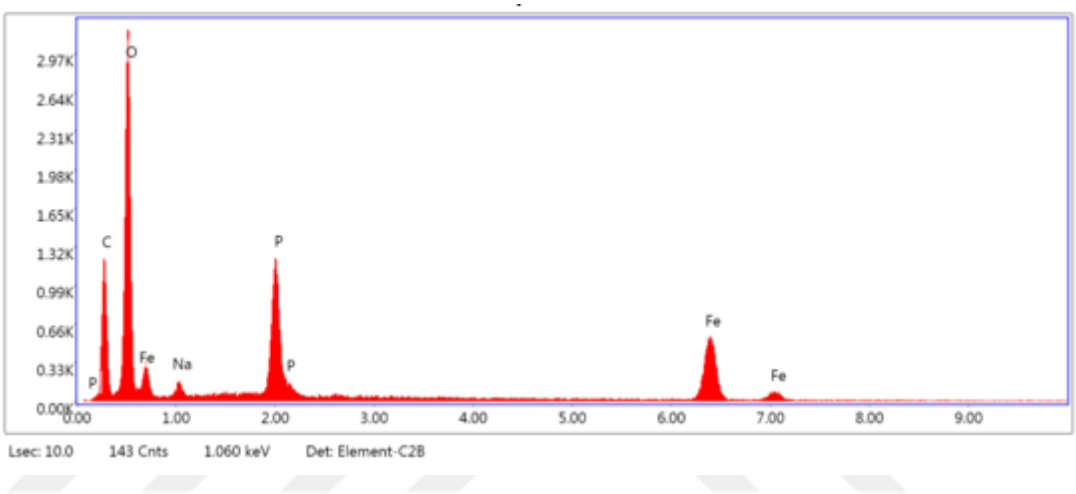

Figure 7.16 SEM-EDX graph of EDS spot 3

Table 7.7 elemental analyses of EDS spot 3

Element	Weight %	Atomic %
C K	22.71	38.45
O K	32.43	41.23
NaK	1.17	1.04
P K	11.55	7.59
FeK	32.13	11.70

7.1.8 Conductivity and pH Changes during Crystallization for CSTR

With the start of the precipitation process, there is a decrease in the types that provide electrical conductivity in the solution, that is, the conductivity decreases. Therefore, it is possible to determine the induction period, which is expressed as the sum of crystal nucleation time and crystal growth time, by using conductivity. For this reason, the conductivity parameter was monitored at regular intervals from the moment the solution containing Fe was mixed by giving it to the reactor until the mixing process was finished. The variation of the conductivity for two trials are given in Figure 7.17, as an example.

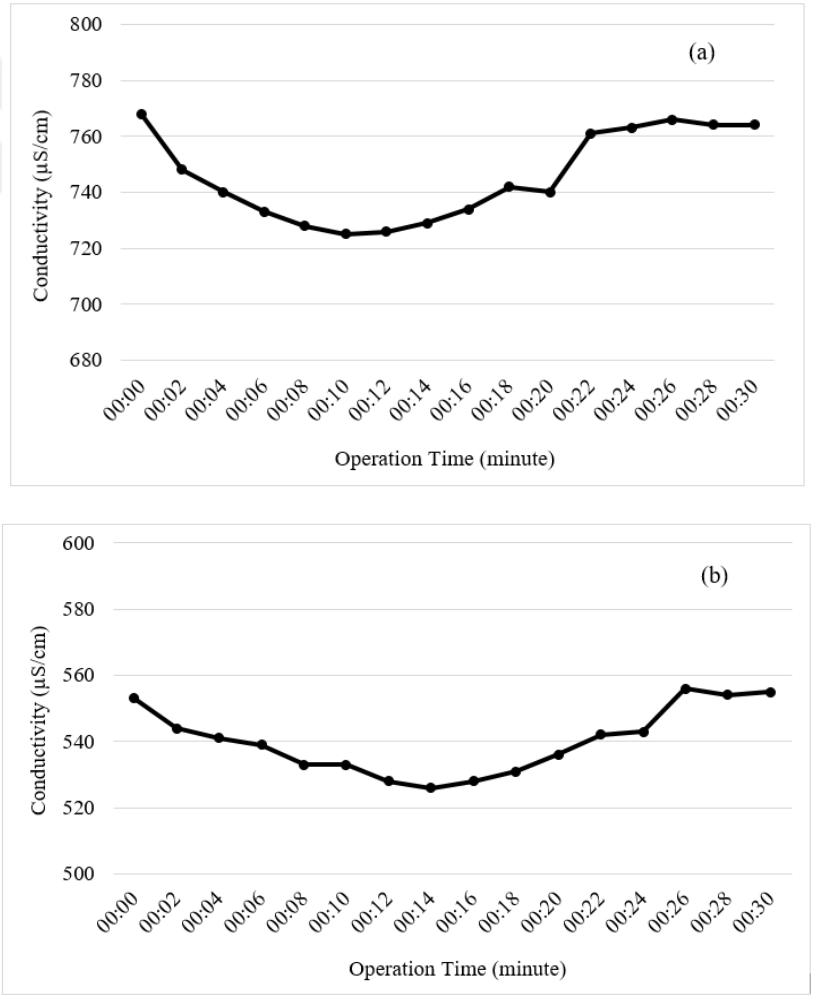

Figure 7.17 The variation of the conductivity for two trials, (a) P = 200 mg/L, Fe:P = 2:1, Fe feeding rate = 2.5 rpm, (b) P = 200 mg/L, Fe:P = 1.5:1, Fe feeding rate = 2.5 rp

For each operating condition, pH analyzes were also performed at the beginning and end of the reaction. The pH values of phosphorus solution prepared with Na_2HPO_4 are around 9.0 ± 0.2 and it was determined around 7.3 ± 0.3 at the end of the reaction. These results showed that the formation of vivianite lowered the pH.

7.2 Fluidized Bed Crystallizer (FBR) Experiments

Before the fluidized bed reactor was started to operate, seed material was added so that a height of 10 cm was obtained in the reactor. There are three flows in total in the fluidized bed reactor trials. Solution containing phosphorus was prepared and fed to the reactor by a peristaltic pump. The iron solution was also prepared to achieve the appropriate Fe:P ratio and was fed to the reactor with a second peristaltic pump. During operation, the fluid level in the reactor was checked regularly. When the fluid level reached the recycle line level, the recycle line was also activated with third peristaltic pump.

The reactor was operated for ninety minutes in all trials. Operation time, Fe:P ratio, water and iron feeding rates have kept constant during the experiments. The highest phosphorus removal (67 %) was obtained for 300 mg/L P concentration. Therefore, detailed calculations and analyses were performed for this experiment. The applied operational conditions and the results of the fluidized bed reactor are shown in Table 7.8. Images of precipitates for 300 mg/L and 500 mg/L P concentration trials are given in Figure 7.18.

Table 7.8 Fluidized bed reactor operational conditions

Initial phosphorus concentration (mg/L)	**Water feed (rpm)**	**Iron feed (rpm)**	**Recycle stream feed (rpm)**	**Phosphorus removal efficiency (%)**
300	15	10	30	67%
500	15	10	20	62%
200	15	10	20	52%

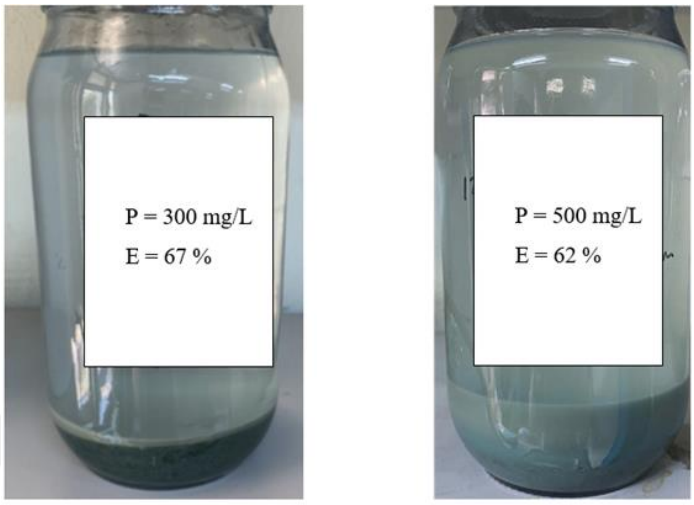

Figure 7.18 Images of precipitates for 300 mg/L and 500 mg/L P concentration (Personal archive, 2022)

Reynold's number was calculated to determine the type of flow. Since it is less than 10, operation of fluidized bed system is less turbulent. Equation 5.4 was used for the calculation of minimum fluidization velocity. It was found as 4.5 m/h. In operational conditions, this value is 5.63 m/h for 30 rpm recycle flow. Finally, pressure drop has been calculated based on Ergun Equation as $3.49x10^5$Pa. Calculations, SEM and SEM-EDS analyses were performed for Experiment Number 1.

7.2.1 SEM Analyses of Fluidized Bed Reactor Samples

Surface morphology of vivianite crystals are characterized by scanning electron microscopy. Samples were taken after 24 h settling time and dried in Nuve EV 018 vacuum oven. The particle size, shape, and surface topography can all be determined using scanning electron microscopy (Zhou & Greer, 2016). SEM analyses were performed at Dokuz Eylül University, Center for Fabrication and Application of Electronic Materials by COXEM EM-30 Plus. Images are shown in Figure 7.19. SEM images were taken changing between x500 to x10000 magnifications with an acceleration voltage of 15-20 kV. Sharp corners of crystals have been seen between 1.5 nm - 3.9 μm in length.

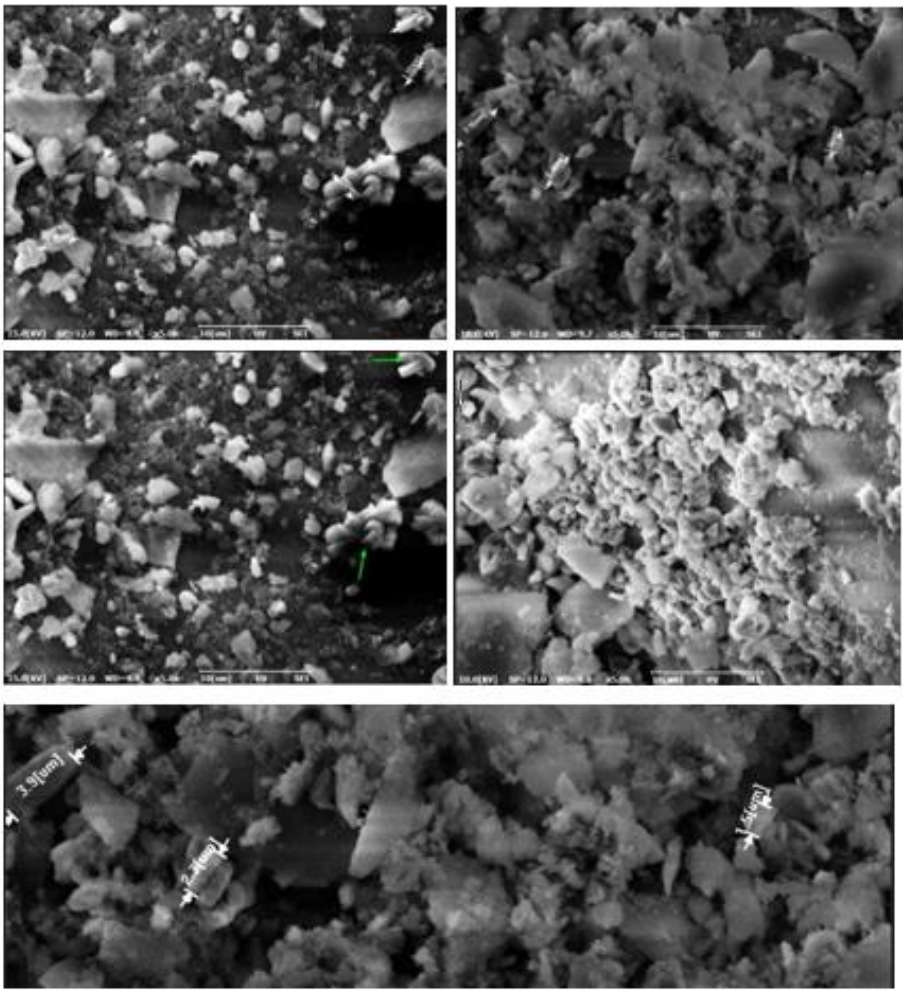

Figure 7.19 SEM images of FBR samples

7.2.2 SEM-EDS Results of Fluidized Bed Crystallizer

SEM-EDX analyzes were performed at Izmir Katip Celebi University. Carl Zeiss 300VP SEM Device was used and elemental analysis of the sample was made with EDX detector. The samples taken from the lower part of the fluidized bed reactor were dried and powdered to examine with the SEM-EDS device for elemental characterization. As in the CSTR reactor trials, it was investigated whether iron and phosphorus elements were formed. Additionally, the Fe:P ratio of synthesized material was examined in terms of atomic mass percentages. Since the Fe:P ratio in the chemical formula of vivianite is 1.5, this value has been taken as a reference in the interpretations.

Five selected were specially investigated in terms of elemental composition. These selected points are shown in Figure 7.20. All graphs and compositions are shown below for each area. Si has been found since the seed material is silica sand.

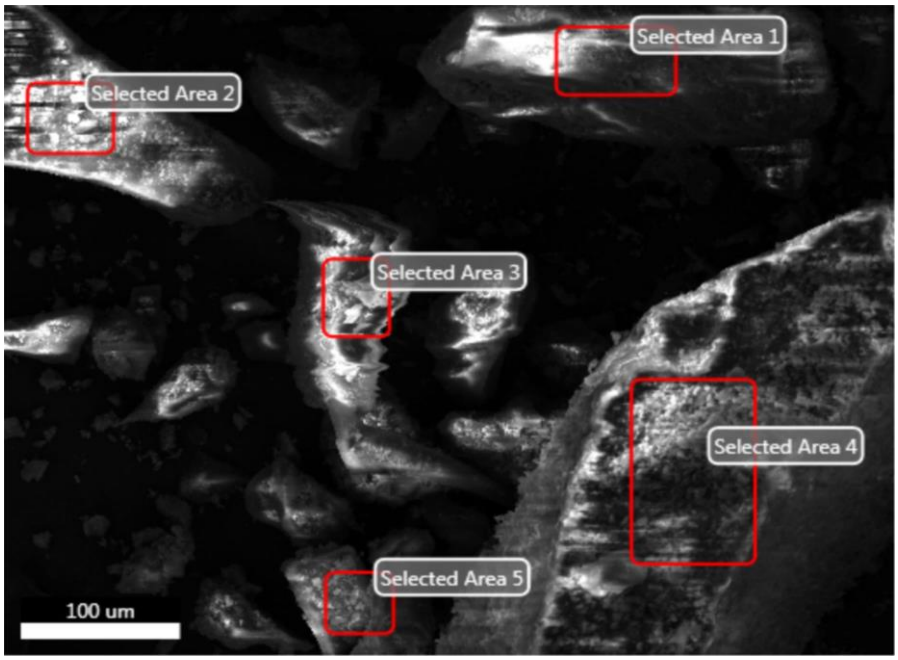

Figure 7.20 SEM-EDS images of FBR samples

Oxygen was observed in all the samples. Anaerobic environment is required for vivianite formation. However, the contact of the samples with oxygen while sampling or measuring may have caused this. The presence of oxygen may be a cause of contamination while taking samples or investigating samples. There are several sources for oxygen, so it is likely to see it in SEM-EDS results. The samples were mainly examined for iron and phosphorus content. Phosphorus and iron, which are expected and desired elements for vivianite formation, have been found in all samples except selected area 4. The closest Fe:P ratio to vivianite is 1.28 which has belonged to selected area 5. Figure 7.21 shows the SEM-EDX graph of selected area 1. Oxygen and silicon elements have highest percentage in this sample. Si element comes from the seed material. Table 7.9 shows the weight and atomic percentages for each element. Iron and phosphorus have 1.36 and 1.41 percentages by atomic mass. The ratio of these elements is 0.96 in this sample.

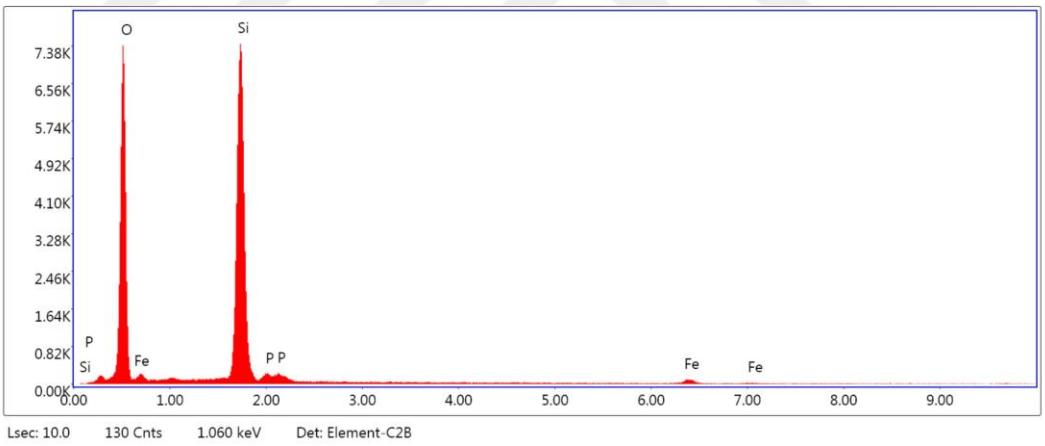

Figure 7.21 SEM-EDX graph of selected area 1

Table 7.9 Elemental analyses of selected area 1

Element	Weight %	Atomic %
O K	51.56	66.11
Si K	42.62	31.13
P K	2.13	1.41
Fe K	3.69	1.36

Figure 7.22 shows the SEM-EDX graph for selected area 2. The most abundant materials in this example are silicon and oxygen. When evaluated over the formation of vivianite, the sample contains iron and phosphorus elements. Weight and atomic percentages of each element is shown in Table 7.10. The Fe:P ratio as atomic mass is 3.

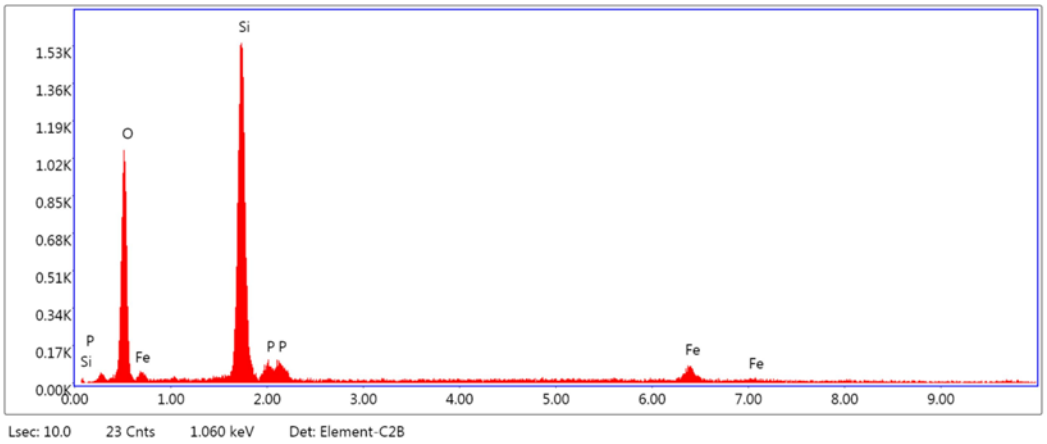

Figure 7.22 SEM-EDX graph of selected area 2

Table 7.10 Elemental analyses of selected area 2

Element	Weight %	Atomic %
O K	36.57	54.10
Si K	42.77	36.04
P K	3.42	2.48
Fe K	17.42	7.38

Figure 7.23 shows the SEM-EDX graph for selected area 3. When the sample is evaluated separately from oxygen and silicon elements, it is seen that it contains iron and phosphorus elements. The abundance of these two elements is quite low for this sample. When analyzed as a percentage of atomic mass, the Fe:P ratio is approximately 1 as shown in Table 7.11.

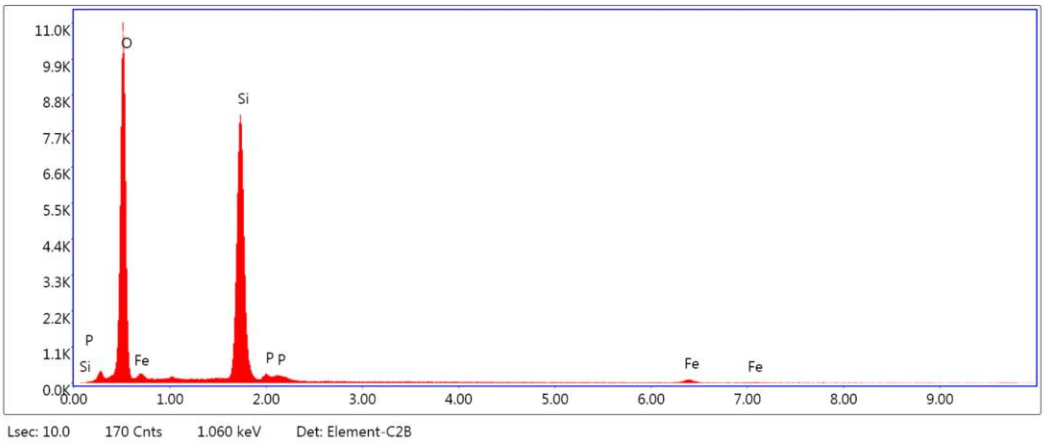

Figure 7.23 SEM-EDX graph of selected area 3

Table 7.11 Elemental analyses of selected area 3

Element	Weight %	Atomic %
O K	57.74	71.40
Si K	34.47	26.39
P K	1.78	1.14
Fe K	3.01	1.07

Figure 7.24 shows the SEM-EDX graph of selected area 4. The sample is consisting of oxygen, sodium, silicon, phosphorus, and iron. Weight and atomic mass percentages of each element is shown in Table 7.12. Sodium is an irrelevant element in terms of aim of the study. Since the amount of its abundance is quite low (1%), it is neglected. Iron and phosphorus elements are present in the sample and Fe:P ratio is 1.10 by atomic mass percentage.

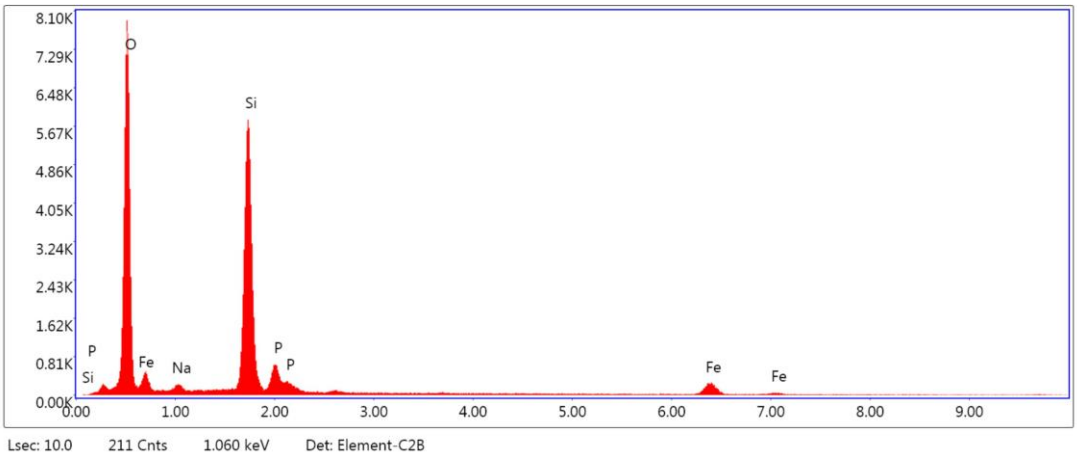

Figure 7.24 SEM-EDX graph of selected area 4

Table 7.12 Elemental analyses of selected area 4

Element	Weight %	Atomic %
O K	49.96	66.49
Na K	1.34	1.24
Si K	31.79	24.10
P K	5.65	3.88
Fe K	11.26	4.29

Figure 7.25 shows the SEM-EDX graph of selected area 5. The sample is consisting of oxygen, silicon, phosphorus, and iron. Weight and atomic mass percentages of each element is shown in Table 7.13. Fe:P ratio is 1.28 by atomic mass percentages.

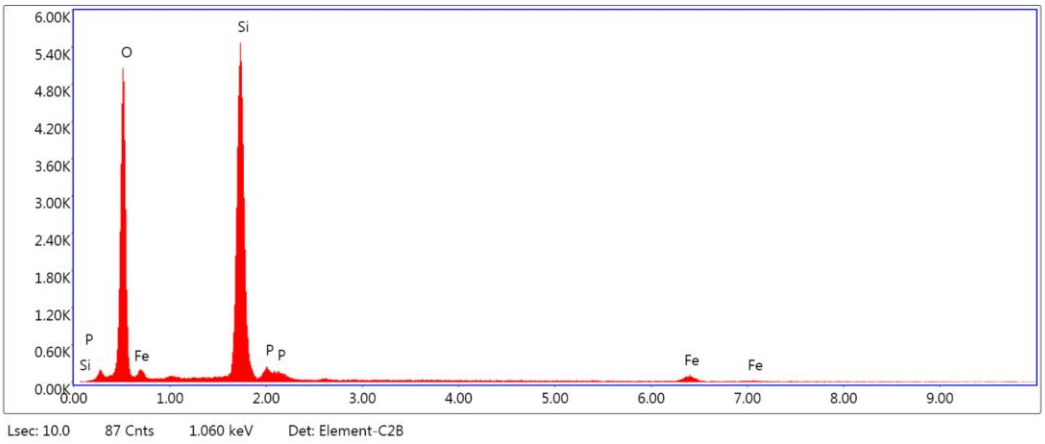

Figure 7.25 SEM-EDX graph of selected area 5

Table 7.13 Elemental analyses of selected area 5

Element	Weight %	Atomic %
O K	48.57	64.01
Si K	42.16	31.65
P K	2.79	1.90
Fe K	6.47	2.44

7.3 Particle Size Distribution

Particle size distribution analysis was made in İzmir Katip Çelebi University Central Research Laboratories by Master sizer hydro 3000 device. Particle size analysis was applied to analyse the particle distribution of the contents in the reactor. The measurement is based on the laser diffraction technique. Graphs are expressed by volumetric distribution.

According to the results, no crystals were observed in volumes below 0.1 µm. The smallest size is approximately 0.6 µm and the largest size is approximately 100 µm. Particles below 45 µm constitute 93.9% of the total volume (Figure 7.26 and 7.27).

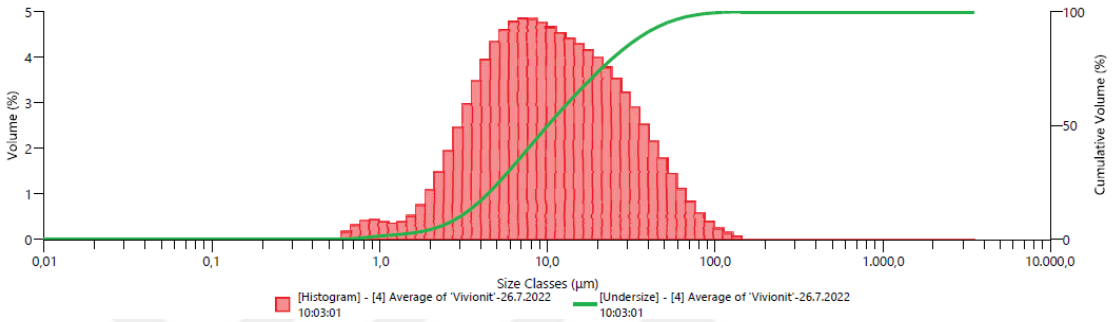

Figure 7.26 Particle size distribution of vivianite in FBR as volume (%)

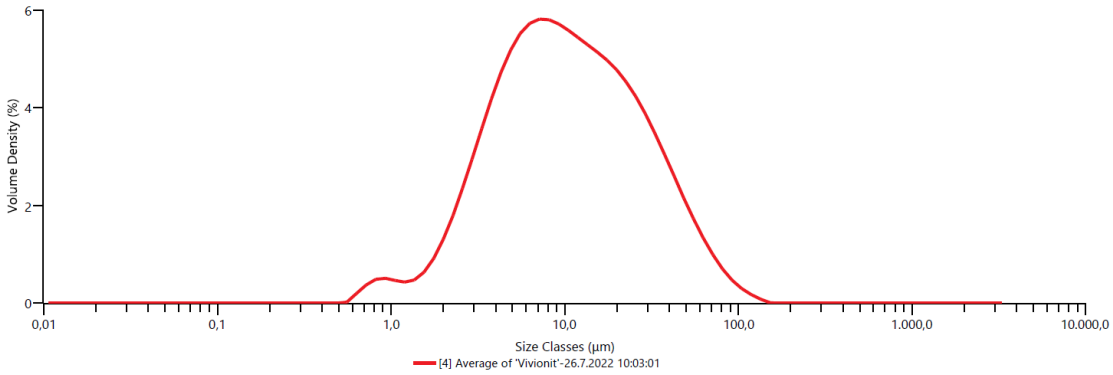

Figure 7.27 Particle size distribution of vivianite in FBR as volume density (%)

CHAPTER 8
CONCLUSION AND RECOMMENDATIONS

In this study, the efficiency of phosphorus recovery from wastewater as vivianite crystal was evaluated. The trials were carried out in two different reactors, CSTR and FBR. To understand the operating system and to determine the factors affecting the formation of vivianite, CSTR trials were first carried out. In FBR trials, the effect of seed material and the use of different P concentrations on crystallization was evaluated. Anaerobic conditions were provided with N_2 gas for two reactors. The conclusions in accordance with this study are summarized below for each type of reactor.

8.1 Fully Mixed (CSTR) Crystallizer

In CSTR trials, the effects of initial phosphorus concentration, Fe:P ratio, iron feed rate, stirrer speed, reaction time, and settling time on vivianite formation were investigated. The following conclusions were obtained:

- The conductivity parameter was monitored throughout the experiment. It was observed that while the conductivity was higher in the first moments of the reaction, it decreased over time. Since the number of free ions in the first moments of the reaction decreased over time, the conductivity parameter decreased. It was observed that the conductivity value was also fixed when the reaction was completed.
- When the yields in the experiments were examined, the highest yields were achieved at pH 7-9. Below or above this range, crystallization formation was not observed frequently. In cases, where formation is observed, the yield is quite low compared to the observations in the pH range of 9-11. It has been determined that the formation of vivianite reduces the pH of the wastewater. The pH value, which was measured in the range of 8-9 at the beginning of the reaction, decreased to the range of 6-7.

- No precipitation was observed when the phosphorus concentration fell below 50 mg/L. Therefore, wastewater with a high phosphorus concentration is more suitable for vivianite crystallization.
- The highest phosphorus recovery was found when the Fe:P ratio was 1.8. Higher phosphorus removal efficiencies were obtained when the Fe:P ratio was close to 2. It is important to achieve the same Fe:P ratio as the chemical formula of vivianite in the reactor.
- Maximum recovery efficiency was achieved at iron feeding rate of 10 rpm. Below or above this value, phosphorus removal efficiency was lower.
- To obtain better crystallization efficiency, the optimum operating time should be determined. For the CSTR trials, the operating time with the highest efficiency were 20 minutes.
- Phosphorus removal for all experiments was measured after a settling time of 24 hours. Below the 24-hour settling time, the results are significantly lower.
- The yields obtained in the CSTR reactor were measured as a maximum of 69%.
- Characterization of the samples were done SEM, XRD and SEM-EDS analysis. Zoomed images of the samples were obtained by SEM analysis. Regular array crystal structures were observed in the images. Crystal structures were investigated by XRD analysis. The peaks in the XRD profile were compared with the results in the databases for vivianite. The peaks obtained in CSTR samples are compatible with databases. Finally, the elemental contents of the samples were examined by SEM-EDS analysis. Since the chemical formula of vivianite $Fe_3(PO_4)_2 \bullet 8(H_2O)$ contains iron and phosphorus elements, SEM-EDS results were evaluated accordingly. Iron and phosphorus were found in the results obtained. When the atomic percentages of the elements were examined, Fe:P ratios were found close to 2, as in the chemical formula of vivianite.

8.2 Fluidized Bed Crystallizer

In the FB reactor trials, the effect of the seed material and P concentrations were determined. The FB reactor was operated in the operating conditions determined according to the results obtained in the CSTR reactor trials. There are three flows in the reactor. The flow that provides fluidization in the reaction zone is the recycle flow. The seed materials were activated by the effect of the upstream velocity of the water and fluidity was observed in the reaction column. Color change started in the column with iron feeding and a blue-green color was observed towards the end of the operation. At the end of the operation, effluent was discharged from the settling zone. Anaerobic environment was created by giving nitrogen gas from the bottom of the reactor at certain time intervals. In accordance with this study, the following conclusions were obtained:

- Calculations were performed based on the Ergun Equation. Minimum fluidization velocity found as 3.99 m/h. In operational conditions this value is 5.63 m/h for 30 rpm recycle flow. Pressure drop has been calculated as $3.49x10^5$Pa.
- The characterization of the samples prepared for FB reactor trials was done by SEM, XRD, and SEM-EDS analyses. Regular crystal arrays were found in the microscope images. The peaks in the XRD graph are compatible with databases. Finally, SEM-EDS graphs were interpreted based on the chemical formula of vivianite, as in the CSTR reactor. In elemental analysis, the presence of iron and phosphorus was observed in the samples. When the Fe:P ratio was examined, results close to 2 were obtained, as in vivianite.
- The phosphorus removal efficiency for FBR trials is 69%. For both reactors, yields are approximately equal.

8.3 Recommendations

As a result of the studies carried out at different phosphorus concentrations, it is determined that the vivianite crystallization process will give higher yields for wastewater with high phosphorus content, such as fertilizer, pharmaceutical, and steel industry wastewater. In domestic wastewater treatment plants, high P content may be found in supernatant of anaerobic digestion. Moragaspitiya et al. (2019) indicated 100–200 mg/L phosphate could be found in supernatant of anaerobic digestion of waste activated sludge. Therefore, the vivianite crystallization process can also be used in here.

When comparing FBR and CSTR operations, cleaning and reloading the CSTR between trials were easier. At the same time, conductivity and pH parameters were easily monitored during the reaction. Reactor cleaning and operation control were more difficult in FBR.

Seed material has a significant effect on crystallization since it helps to provide a surface for crystallization. In FBR trials, silica sand was used as seed material. Since seed material was used, better phosphorus removal efficiency was expected. However, phosphorus efficiencies are almost the same as for FBR and CSTR experiments. For this reason, the efficiency of using different seed materials such as pumice, zeolite, etc. on crystallization can be investigated.

Although many operating conditions have been tested in the scope of this thesis, similar additional studies are required for more efficient phosphorus recovery. It is important for sustainable P management to conduct research on the use of vivianite as fertilizer or its use in industry in future studies.

REFERENCES

Antoniewicz, P. (2021, May 29). *Understanding and coping with struvite/vivianite formation in wwtps.* Water Online. https://www.wateronline.com/doc/understanding-and-coping-with-struvite-vivianite-formation-in-wwtps-0001

Atalay, Z. (2006). *Yabancı iyonların struvit çöktürmesi kinetiği üzerine etkilerinin araştırılması* [Master's Thesis]. İstanbul Technical University.

Banerjee, D. (2022, August 3). *X-Ray diffraction (XRD).* IIT Kanpur. https://www.iitk.ac.in/che/pdf/resources/XRD-reading-material.pdf

Binev, D. (2015). *Continuous fluidized bed crystallization* [Ph.D. Thesis]. Otto-von-Guericke-Universität Magdeburg.

Cieślik, B., & Konieczka, P. (2017). A review of phosphorus recovery methods at various steps of wastewater treatment and sewage sludge management. The concept of "no solid waste generation" and analytical methods. *Journal of Cleaner Production*, *142*, 1728-1740.

Cordell, D., & White, S. (2011). Peak phosphorus: clarifying the key issues of a vigorous debate about long-term phosphorus security. *Sustainability*, *3*(10), 2027-2049.

Cordell, D., & White, S. (2014). Life's bottleneck: sustaining the world's phosphorus for a food secure future. *Annual Review of Environment and Resources*, *39*, 161-188.

Cornel, P., & Schaum, C. (2009). Phosphorus recovery from wastewater: needs, technologies and costs. *Water Science and Technology*, *59*(6), 1069-1076.

Curtin, K., Duerre, S., Fitzpatrick, B., Meyer, P., & Ellefson, N. (2011). *Biological Nutrient Removal.* The Minnesota Pollution Control Agency https://www.pca.state.mn.us/sites/default/files/wq-wwtp8-21.pdf

Doğan, F. (2010). *Mevcut atıksu arıtma tesislerinin fosfor giderimi için rehabilitasyonunda seçeneklerin değerlendirilmesi* [Specialist thesis]. Çevre Yönetimi Genel Müdürlüğü Su ve Toprak Yönetimi Dairesi Başkanlığı

Dorofeev, A. G., Nikolaev, Y. A., Mardanov, A. V., & Pimenov, N. V. (2020). Role of phosphate-accumulating bacteria in biological phosphorus removal from wastewater. *Applied Biochemistry and Microbiology, 56*(1), 1-14.

Eskier, U. (2021, April 11). *Fosfor Nedir, Nerelerde Kullanılır?.*Makaleler. https://www.makaleler.com/fosfor-nedir-nerelerde-kullanilir

Fodoué, Y., Nguetnkam, J. P., Tchameni, R., Basga, S. D., & Penaye, J. (2015). Assessment of the fertilizing effect of vivianite on the growth and yield of the bean 'Phaseolus vulgaris' on oxisoils from Ngaoundere (central north Cameroon). *Int. Res. J. Earth Sci*, *3*(4), 18-26.

Geankoplis, C. J. (2003). Transport processes and separation. In *Process Principles*. Prentice Hall NJ.

Janson, J. (2021). *Vermeer's palette: Rare or unidentifiable pigments (Schijtgeel & Vivianite).* Rare or Unidentifiable Pigments: Schijtgeel & Vivianite. Retrieved November 2, 2022, from http://www.essentialvermeer.com/palette/rare.html

Jupp, A. R., Beijer, S., Narain, G. C., Schipper, W., & Slootweg, J. C. (2021, January 7). Phosphorus recovery and recycling-closing the loop. *Chemical Society Reviews*. https://doi.org/10.1039/d0cs01150a

Kentsel atıksu yönetmeliği. (2021, January 8). *Resmi Gazete.* https://www.mevzuat.gov.tr/mevzuat?MevzuatNo=9844&MevzuatTur=7&MevzuatTertip=5

Kok, D. J. D., Pande, S., Van Lier, J. B., Ortigara, A. R., Savenije, H., & Uhlenbrook, S. (2018). Global phosphorus recovery from wastewater for agricultural reuse. *Hydrology and Earth System Sciences, 22*(11), 5781-5799.

Le Corre, K. S., Valsami-Jones, E., Hobbs, P., & Parsons, S. A. (2009). Phosphorus recovery from wastewater by struvite crystallization: A review. *Critical Reviews in Environmental Science and Technology, 39*(6), 433-477.

Lee, M. (2021, October 21). *Fluidized bed crystallization (fbc) wastewater treatment technology*. Itri Water. https://www.itriwater.org.tw/Eng/technology/More?id=97

Lewis, A., Seckler, M., Kramer, H., & Van Rosmalen, G. (2015). *Industrial crystallization: fundamentals and applications*. Cambridge University Press. https://doi.org/10.1017/CBO9781107280427

Liu, J., Cheng, X., Qi, X., Li, N., Tian, J., Qiu, B., … Qu, D. (2018). Recovery of phosphate from aqueous solutions via vivianite crystallization: Thermodynamics and influence of pH. *Chemical Engineering Journal, 349*, 37–46.

Madhu (2021, December 31). *Difference between homogeneous and heterogeneous nucleation.* Difference Between. https://www.differencebetween.com/difference-between-homogeneous-and-heterogeneous-nucleation/

Ministry of Agriculture and Forestry (2021, April 4). ZMO: *Ülkemizde gübre üretimi ve tüketimi üzerine bir değerlendirme.* TMMOB. https://www.tmmob.org.tr/icerik/zmo-ulkemizde-gubre-uretimi-ve-tuketimi-uzerine-bir-degerlendirme

Moragaspitiya, C., Rajapakse, J., Millar, G. J., & Ali, I. (2019). Optimization of mesophilic anaerobic digestion of a conventional activated sludge plant for sustainability. *Alexandria Engineering Journal, 58*(3), 977-987.

N.d. (2021, October 21). *Vivimag.* Wetsus.

https://www.wetsus.nl/project/vivimag/

N.d (2021, April 24). *The phosphorus cycle*. Science Learning Hub. https://www.sciencelearn.org.nz/resources/961-the-phosphorus-cycle

N.d. (2022, August 11). *SEM - Scanning Electron Microscope*. Westmorland. https://www.wmtr.com/en.SEM.html#pa

N.d. (2021, June 20). *Vivianite: mineral information, data and localities.* Mindat. https://www.mindat.org/min-4194.html

N.d. (2022, August 15). *Electricity prices around the world.* Global Petrol Prices. https://www.globalpetrolprices.com/electricity_prices/? s=09

N.d. (2021, December 30). *Crystallization.* Reciprocal Net. http://www.reciprocalnet.org/edumodules/crystallization/index.html

N.d. (2021, April 24). *Fosfat Kayası*. Eti Bakır. https://etibakir.com.tr/urunler/fosfat-kayasi/

Pakdil, N. B., & Filibeli, A. (2008). The evaluation of pumice stone applicability at struvite crystallization by using Box–Benhken experimental design. *J. Residuals Sci. Technol*, *5*(2), 95-102.

Pathak, B. (2021, June 6). *Vivianite impacts on solids processes.* WEF. https://www.wef.org/globalassets/assets-wef/3---resources/topics/an/biosolids/technical-resources/005-vivianite-impacts-on-solids-processes-final.pdf

Prot, T., Korving, L., Dugulan, A. I., Goubitz, K., & van Loosdrecht, M. C. M. (2021). Vivianite scaling in wastewater treatment plants: Occurrence, formation mechanisms and mitigation solutions. *Water Research*, *197*, 117045.

Prot, T., Nguyen, V. H., Wilfert, P., Dugulan, A. I., Goubitz, K., De Ridder, D. J., … van Loosdrecht, M. C. M. (2019). Magnetic separation and characterization of vivianite from digested sewage sludge. *Separation and Purification Technology*, *224*, 564–579. https://doi.org/10.1016/j.seppur.2019.05.057

Reta, G., Dong, X., Li, Z., Su, B., Hu, X., Bo, H., ... & Xu, S. (2018). Environmental impact of phosphate mining and beneficiation: review. *International Journal of Hydrology*, *2*(4), 424-431.

Rothe, M., Frederichs, T., Eder, M., Kleeberg, A., & Hupfer, M. (2014). Evidence for vivianite formation and its contribution to long-term phosphorus retention in a recent lake sediment: a novel analytical approach. *Biogeosciences, 11*(18), 5169-5180. https://doi.org/10.5194/bg-11-5169-2014

Rothe, M., Kleeberg, A., & Hupfer, M. (2016). The occurrence, identification, and environmental relevance of vivianite in waterlogged soils and aquatic sediments. *Earth-Science Reviews, 158*, 51-64.

Rothe, M., Kleeberg, A., Grüneberg, B., Friese, K., Pérez-Mayo, M., & Hupfer, M. (2015). Sedimentary sulphur:iron ratio indicates vivianite occurrence: A study from two contrasting freshwater systems. PLoS ONE, 10(11). https://doi.org/10.1371/journal.pone.0143737

Royal Society of Chemistry. (2021, April 18). *Phosphorus - element information properties and uses: Periodic Table. Phosphorus - Element information, properties and uses Periodic Table.* RSC. https://www.rsc.org/periodic-table/element/15/phosphorus

Raman, X-ray, Infrared, and Chemistry. (2022, August 3*). Vivianite R07033.* RRUFF. https://rruff.info/Vivianite/R070331

South-Eastern Finland University of Applied Sciences. (2021, January 19). *Uses and advantages of crystallization*. Share and Discover Knowledge on SlideShare. Retrieved November 2, 2022, from https://www.slideshare.net/Xamk/uses-and-advantages-of-crystallization?next_slideshow=241554636

Schönberg, A., Raupenstrauch, H., & Ponak, C. (2018). Recovery of phosphorus in sewage sludge treatment. *Universal Medien GmbH, Munich*

Suleiman, Y., Ibrahim, H., Anyakora, N. V., Mohammed, F., Abubakar, A., Aderemi, B. O., & Okonkwo, P. C. (2013). Design and fabrication of fluidized-bed reactor. *International Journal of Engineering and Computer Science*, *2*(5), 1595-1605.

TAGEM. (2022). *Gübre Sektör Politika Belgesi 2018-2022.* Tarım Orman. https://www.tarimorman.gov.tr/TAGEM/Belgeler/yayin/G%C3%BCbre%20Sekt%C3%B6r%20Politika%20Belgesi%202018-2022.pdf

Water Environment Federation. (2011). *Nutrient Removal - Manual of Practice*. McGraw Hill.

Wilfert, P., Dugulan, A. I., Goubitz, K., Korving, L., Witkamp, G. J., & Van Loosdrecht, M. C. M. (2018). Vivianite as the main phosphate mineral in digested sewage sludge and its role for phosphate recovery. *Water research*, *144*, 312-321.

Wu, G., Zeng, W., Li, S., Jia, Z., & Peng, Y. (2021). Phosphorus recovery from waste activated sludge by sponge iron seeded crystallization of vivianite and process optimization with response surface methodology. *Environmental Science and Pollution Research*, *28*(41), 58375-58386.

Wu, Y., Luo, J., Zhang, Q., Aleem, M., Fang, F., Xue, Z., & Cao, J. (2019, July 1). Potentials and challenges of phosphorus recovery as vivianite from wastewater: A review. *Chemosphere. Elsevier Ltd.* https://doi.org/10.1016/j.chemosphere.2019.03.138

Yin, Z., Fu, Y., & Chen, Q. (2019). Research progress in recovering phosphorus from wastewater by crystallization. *In E3S Web of Conferences* (*Vol. 118*, p. 04031). EDP Sciences.

Zhou, W., & Greer, H. F. (2016). What can electron microscopy tell us beyond crystal structures?. *European Journal of Inorganic Chemistry*, *2016*(7), 941-950.